Journal of Macromolecular Science, Part A
Publication details, including instructions for authors and subscription information:
http://www.informaworld.com/smpp/title~content=t713597274

Particle Formation in Emulsion Polymerization: Particle Number at Steady State

Z. Song[a]; G. W. Poehlein[a]
[a] School of Chemical Engineering Georgia Institute of Technology, Atlanta, Georgia

To cite this Article Song, Z. and Poehlein, G. W.(1988) 'Particle Formation in Emulsion Polymerization: Particle Number at Steady State', Journal of Macromolecular Science, Part A, 25: 12, 1587 — 1632
To link to this Article: DOI: 10.1080/10601328808055090
URL: http://dx.doi.org/10.1080/10601328808055090

J. MACROMOL. SCI.—CHEM., A25(12), pp. 1587-1632 (1988)

PARTICLE FORMATION IN EMULSION POLYMERIZATION: PARTICLE NUMBER AT STEADY STATE

Z. SONG and G. W. POEHLEIN

School of Chemical Engineering
Georgia Institute of Technology
Atlanta, Georgia 30332-0100

ABSTRACT

The number of particles formed in batch emulsion polymerization over wide ranges of emulsifier and initiator concentration has been investigated by computer simulation with a mathematical model developed in a previous paper. The influence of particle coagulation is also considered. The results show that, at low emulsifier concentration, the steady-state particle number N_s is governed by homogeneous nucleation so that N_s increases slowly with increasing emulsifier concentration [S]. In this range, N_s increases with increasing monomer polarity. The steep rise in N_s with emulsifier concentration after [S] exceeds a critical value suggests a transition from homogeneous nucleation domination to micelle nucleation. The slope of the N_s vs [S] relationship increases as the particle coagulation rate constant K_f increases. The power x in the empirical relationship $N_s \approx [S]^x$ decreases with increasing polarity of monomer in this region. At very high micelle concentration, insufficient radical generation and the increasing tendency for particle coagulation cause N_s to be less dependent on emulsifier concentration. These phenomena have been reviewed by Vanderhoff and confirmed by the experimental data presented by Sutterlin. The particle number increases with increasing initiator concentration [I] when [S] is above the CMC. As [I] continues to increase, however, N_s becomes relatively constant. Experimental data for styrene, butyl acrylate, and methyl acrylate from the literature are compared with the model predictions.

Agreement between the theoretical predictions and the experimental data is evident over a wide range of emulsifier and initiator concentrations.

INTRODUCTION

Smith and Ewart [4] proposed the following simple relationship for the final particle number, N_s, in emulsion polymerization:

$$N_s = K(\rho_i/\mu)^{0.4}(a_s[\mathrm{S}])^{0.6}, \tag{1}$$

where K is a constant, equal to 0.37 for the lower limit and 0.53 for the upper limit, μ is a constant rate of increase in the volume of each particle; a_s is the interfacial area occupied by a mole of emulsifier, [S] is the molar emulsifier concentration, and ρ_i is the initiation rate. Equation (1) has often formed the basis of a test of the applicability of the Smith-Ewart theory in emulsion polymerization. Some results (most are for styrene) were in agreement with the theory, but others were not. An exponent of 0.5 has been reported by Breitenbach and Edelhauser [5], Morton and Landfield [6], and Friis and Nyhagen [7] for the dependence of N_s on [S]. Chen and Chang [8] as well as Chatterjee and Banerjee [9] have reported a 0.5 exponent for initiator concentration, [I], even for the styrene monomer systems. Zollars [10] and Friis and Nyhagen [7] have reported some cases in which N_s was independent of initiator concentration. Zollars [10] reported that the power relationship between N_s and [I] changed with the magnitude of [I] as well as with temperature for the emulsion polymerization of vinyl acetate.

In general, the Smith-Ewart theory is believed to be applicable to monomers with limited water solubility, such as styrene. Vinyl acetate and methyl methacrylate are not commonly observed to follow Smith-Ewart kinetics because of their relatively high solubilities in water and for other reasons, such as the gel effect and radical desorption. However, data from the emulsion polymerization of monomers whose water solubilities are less than that of styrene do not follow the Smith-Ewart theory. Moore [11] investigated the emulsion polymerization of a very sparingly water-soluble monomer, vinyl stearate (water solubility 7×10^{-7} mol/L compared with that of styrene 3.5×10^{-3} mol/L). He reported that the particle number N_s was independent of initiator concentration. N_s increased with emulsifier concentration [S], but no linear relation was observed between $\log N_s$ and $\log$ [S], as is predicted by Eq. (1). Piirma [12], using mixed emulsifiers, also noticed that

the data for styrene emulsion polymerization did not fall on a straight line on the plot of $\log R_p$ vs $\log$ [S]. Gerrens and Kohnlein [13] reported, for the emulsion polymerization of 2,4-dimethylstyrene (whose solubility in water is supposed to be less than that of styrene), a dependence of N_s on the first power of [S] and on the 0.08 power of initiator concentration [I]. Thus, it can be seen that the relationship between N_s and [S] and ρ_i can be complex for different monomers and under different reaction conditions.

Sutterlin [3] carried out experiments with a series of acrylates, methacrylates, and also styrene to investigate the influence of monomer polarity on particle formation. He observed three regions on the N_s [S] curves.

1st region: At emulsifier concentrations markedly below the CMC, very little soap is available for stabilization of the oligomer radicals. In this range the higher self-stabilization of the polar monomers and their more rapid rate of particle formation in the homogeneous phase dominates. The number of particles formed per unit volume thus increases with increasing monomer polarity.

2nd region: Near the CMC the availability of emulsifier is drastically increased. This is of particular benefit to nonpolar monomers which, due to their moderate self-stabilization and poor water solubility, do not readily form particles in the homogeneous phase. The result is a steep rise of the $N_s = f([S])$ function in the vicinity of the CMC.

3rd region: At soap concentrations noticeably above the CMC, sufficient soap is available to cover the internal surface of the system. Since hydrophobic interfaces are more densely covered with soap, they are also better stabilized. Such systems show a reduced agglomeration tendency and, therefore, their particle number increases more steeply with the soap concentration than that of more polar monomers.

Sutterlin et al. [3, 14] found that the exponent x of the function $N_s \approx [S]^x$ decreases with increasing monomer polarity above the CMC.

Vanderhoff [2] summarized previous work and presented a typical variation of N_s with emulsifier concentration, as shown in Fig. 1. At emulsifier concentrations well below the CMC, N_s increases slowly at first and then more rapidly, until it rises almost vertically at the CMC, to level off at an emulsifier concentration well above the CMC. The near-horizontal part of the curve at very low emulsifier concentration suggests that initiation in the aqueous phase is the principal mechanism of particle nucleation and that N_s is determined more by the stabilizing effect of the sulfate end groups introduced by the persulfate initiator than by the adsorption of emulsifier.

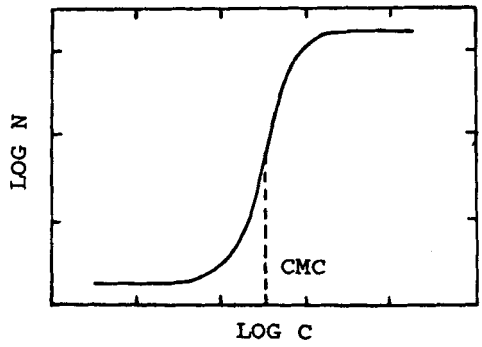

FIG. 1. Typical variation of the number of particles with emulsifier concentration [2].

The near-horizontal curve at emulsifier concentrations well above the CMC suggests that, here, N_s is determined more by the rate of radical generation than by the number of micelles. Vanderhoff postulated that the steep rise in N_s near the CMC might result from the formation of emulsifier aggregates (micelles) at concentrations well below the CMC.

Recently, Lichti, Gilbert, and Napper [15] observed from the positively skewed plot of particle size distribution (PSD) that the rate of production of new latex particles increased during much of the nucleation period. To explain this, Lichti et al. [15] and Feeny et al. [16] proposed a two-step coagulative nucleation model, according to which the "true" (i.e., mature) latex particles are formed through coagulation of so-called "precursor particles" rather than through growing of the precursor particles by polymerization. The precursor particles can be formed, in turn, by the homogeneous nucleation or by micelle-entry nucleation. The precursor particles are colloidally unstable because of their small size (<5 nm).

Feeny et al. [16] determined the steady-state (or final) particle number with the two-step coagulative model by assuming that the formation of new precursor particles ceases when there is no longer any free surfactant to stabilize them, the same assumption used by Smith and Ewart [4].

Napper and Gilbert [17] pointed out that "to-date, coagulative nucleation theory has only been applied to styrene emulsion polymerizations. Whether it is applicable to the emulsion polymerization of other monomers remains to be determined experimentally."

Dunn and Hassan [18] carried out emulsion polymerization of styrene

using Aerosol MA or Lankropol KMA as emulsifier, also finding S-shaped N_s vs [S] curves. Dunn and Hassan believed that micellar nucleation dominated when the emulsifier concentration was above the CMC. However, coagulation was important and coagulative nucleation might operate at emulsifier concentration below the CMC. The constant particle number achieved in emulsion polymerization with emulsifier concentration either above or below the CMC might actually result from a steady state in which the rate of particle formation happens to balance that of particle coagulation.

The mechanisms of particle nucleation in emulsion polymerization were discussed, and a mathematical model was proposed in a previous paper [1]. A three-parameter analytical solution was obtained from this model for the dynamics of the particle number N during the transient portion of batch emulsion polymerization. In this paper, model predictions of the particle number at the steady state, N_s, will be examined by computer simulation. Experimental data from the literature are used for comparison with the model predictions.

THEORY

The following equation for particle generation rate in emulsion polymerization was developed in a previous paper [1]:

$$d[\mathrm{P}]/dt = b\rho_i - K_c B B_i [\mathrm{P}] - K_f [\mathrm{P}]^2, \tag{2}$$

where [P] is the particle concentration, b is a parameter which accounts for aqueous phase termination, and ρ_i is the initiation rate of oligomeric radicals in the aqueous phase. K_c is the average rate constant of radical capture by particles and is defined by

$$K_c = \sum_{i=1}^{\infty} \frac{K_{ci}[\mathrm{P}_i]}{[\mathrm{P}]}, \tag{3}$$

where $[\mathrm{P}_i]$ is the concentration of particles of size i, [P] is the total particle concentration defined by $[\mathrm{P}] = \sum_{i=1}^{\infty} [\mathrm{P}_i]$, and K_{ci} is the rate constant of radical capture by particles of size i. K_f in Eq. (2) is the average coagulation constant of particles and is defined by

$$K_f = \frac{(1/2)\sum_{i=1}^{\infty}\sum_{j=1}^{\infty} K_{fij}[P_i][P_j] + (1/2)\sum_{i=1}^{\infty} K_{fi}[P_i]^2}{[P]^2}, \quad (4)$$

where K_{fij} is the coagulation constant between particles of size i and j. The parameters B_i, B, and b are defined by the following equations:

$$B = \frac{\alpha_p(1 - \alpha_p^{n^*-1})}{k_p M_w(1 - \alpha_p)}, \quad (5)$$

$$B_i = 1 + \rho_{ia}/\rho_i + \rho_{im}/\rho_i + (K_e f_e \bar{n}[P]N_A)/\rho_i, \quad (6)$$

$$b = 1 - (1 - C)k_{tw}B^2 B_i^2 \rho_i, \quad (7)$$

$$C = \frac{\alpha_p^{n^*-2}}{(1 - \alpha_p^{n^*-1})^2}[n^* - 1 - n^*\alpha_p - n^*\alpha_p^{n^*-2} + 2n^*\alpha_p^{n^*-1} - (n^* - 1)\alpha_p^{n^*}], \quad (8)$$

where k_p is the propagation rate constant; M_w is the monomer concentration in the aqueous phase; k_{tw} is the termination rate constant in the aqueous phase; ρ_{ia} and ρ_{im} are the rates of chain transfer to chain transfer agent (CTA) and to monomer, respectively; $\rho_e = K_e f_e \bar{n}[P]N_A$ is the rate of radical desorption from particles; K_e is a desorption rate constant; $\bar{n}$ is the average number of radicals per particle; N_A is Avogadro's number; f_e is the fraction of radicals in the particle phase ($\bar{n}[P]N_A$) that can be desorbed; n^* is the critical chain length above which an oligomer will precipitate from the aqueous phase, and α_p is defined by

$$\alpha_p = \frac{k_p M_w}{k_p M_w + K_{mc}[Mc] + K_{md}[Md] + K_c[P] + k_{tw}[R_w] + k_{tr}[CTA]_w + k_{trm}M_w}, \quad (9)$$

where [Mc], [Md], and $[CTA]_w$ are the concentrations of micelles, monomer droplets, and chain-transfer agent, respectively; K_{mc} and K_{md} are the rate constants for radical capture by micelles and monomer droplets; and k_{tr} and k_{trm} are the rate constants for chain transfer to chain transfer agent and monomer. $[R_w]$ is the total radical concentration in the aqeuous phase. The following aqeuous-phase balance equations for the total radicals and individual radicals with chain length i, $[M_i]$, are used to determine $[R_w]$. The assumption of a steady-state free radical concentration is employed.

$$\frac{d[R_w]}{dt} = \rho_i + \rho_e - k_p M_w [M_{n^*-1}] - \{K_{mc}[Mc] + K_{md}\}[Md] + K_c[P]\,[R_w]$$
$$- 2k_{tw}[R_w]^2 - k_{tr}[CTA]_w[R_w] + k_{ia}M_w[A\cdot] = 0, \quad (10)$$

$$\frac{d[M_1]}{dt} = \rho_i + \rho_{el} - \{k_p M_w + K_{mc}[Mc] + K_{md}[Md] + K_c[P]\}[M_l]$$
$$- 2k_{tw}[R_w][M_1] - k_{tr}[CTA]_w[M_1] + k_{ia}M_w[A\cdot]$$
$$+ k_{trm}M_w \sum_{m=2}^{n^*-1}[M_m] = 0, \quad (11)$$

$$\frac{d[M_m]}{dt} = k_p M_w [M_{m-1}] - \{k_p M_w + K_{mc}[Mc] + K_{md}[Md]$$
$$+ K_c[P]\}[M_m] - k_{tw}[R_w][M_m] - k_{tr}[CTA]_w[M_m] + \rho_e f_{em} = 0, \quad (12)$$

$$\frac{d[A\cdot]}{dt} = k_{tr}[CTA]_w[R_w] - k_{ia}M_w[A\cdot] = 0, \quad (13)$$

where $[A\cdot]$ is the concentration of chain-transfer agent radicals in the aqueous phase, k_{ia} is the reinitiation rate constant for monomer by the chain-transfer agent radicals, and f_{em} is the fraction of desorbed radicals with chain length m. Equations (11) and (12) can be written as follows at the steady state:

$$[M_1] = \frac{\rho_i + \rho_{ia} + \rho_{im} + \rho_e f_{el}}{k_p M_w}, \quad (14)$$

$$[M_m] = \alpha_p \{[M_{m-1}] + \rho_e f_{em}/(k_p M_w)\} \qquad (m = 2, 3, \ldots, n^* - 1), \quad (15)$$

where ρ_{ia} and ρ_{im}, the rates of chain transfer to CTA and monomer, respectively, are defined by

$$\rho_{ia} = k_{tr}[CTA]_w[R_w] \quad (16)$$

$$\rho_{im} = k_{trm}M_w[R_w] \quad (17)$$

Assuming that only monomer radicals (i.e., M_1) can be desorbed from particles, combination of Eqs. (14) and (15) then yields

$$[M_m] = \alpha_p{}^m \frac{\rho_i + \rho_{ia} + \rho_{im} + \rho_e f_{el}}{k_p M_w} \quad (m = 1, 2, \ldots, n^* - 1). \tag{18}$$

Thus,

$$[R_w] = \sum_{m=1}^{n^*-1} [M_m] = \alpha_p \frac{(1 - \alpha_p{}^{n^*-1})(\rho_i + \rho_{ia} + \rho_{im} + \rho_e f_{el})}{(1 - \alpha_p)(k_p M_w)}. \tag{19}$$

Substituting Eqs. (13), (18), and (19) into Eq. (10) and rearranging yields

$$D_1(1 - \alpha_p{}^{n^*-1})[\alpha_p/(1 - \alpha_p)]^2 + D_2\alpha_p/(1 - \alpha_p) - 1 = D_3/(1 - \alpha_p{}^{n^*-1}), \tag{20}$$

where

$$D_1 = \frac{K_{tw}(\rho_i + \rho_{ia} + \rho_e f_{el})}{(k_p M_w)^2}, \tag{21}$$

$$D_2 = \frac{K_{mc}[Mc] + K_{md}[M_d] + K_c[P]}{k_p M_w}, \tag{22}$$

$$D_3 = \frac{\rho_{ia} + \rho_{im}}{\rho_i + \rho_{ia} + \rho_{im} + \rho_e f_{el}}. \tag{23}$$

The particle concentration at the steady state, $[P]_s$, can be determined by setting $d[P]/dt = 0$ in Eq. (2) and solving for $[P]_s$:

$$[P]_s = \frac{\rho_i K_c B B_i}{2K_f}\left\{\sqrt{1 + \frac{4bK_f}{\rho_i(K_c B B_i)^2}} - 1\right\}. \tag{24}$$

COMPUTER SIMULATION

The key point in determining $[P]_s$ with Eq. (24) is to estimate α_p so that B and b can be calculated by Eqs. (5) and (7), respectively. The defining equation, Eq. (9), shows that α_p can be considered to be the probability of homogeneous propagation of radicals in the aqueous phase. α_p can be determined with Eq. (20). When chain transfer reactions can be neglected (i.e., $\rho_{ia} = \rho_{im} = 0$), $D_3 = 0$ and Eq. (20) can be reduced to

$$D_1 \alpha_p^{n^*-1} + (1 + D_2 - D_1)\alpha_p^2 - (D_2 + 2)\alpha_p + 1 = 0. \tag{25}$$

If $\alpha_p^{n^*-1} \ll 1$, $(1 - \alpha_p^{n^*-1}) = 1$ and Eq. (25) can be solved for α_p:

$$\alpha_p = \frac{\sqrt{D_2^2 + 4D_1} - D_2}{\sqrt{D_2^2 + 4D_1} - D_2 + 2D_1}. \tag{26}$$

In the following computer simulation, values of α_p calculated by Eq. (26) are used as initial values for solving Eq. (25) for the true values of α_p by Newtonian iteration.

The computer simulation is for the situation where chain-transfer reactions and the desorption of radicals from particles can be neglected, i.e., $\rho_{ia} = \rho_{im} = \rho_e = 0$ (though this situation does not hold for VA and VCl systems). Thus, D_1 is calculated by

$$D_1 = \frac{k_{tw}\rho_i}{(k_p \mathrm{M}_w)^2}. \tag{27}$$

In the model simulation, D_2 is assumed to be constant since micelles and monomer droplets are transformed into particles. Note the decrease in [Mc] and [Md] is only partially compensated for by the increase in [P] but, as has shown by Fitch and Tsai [19], K_c should be greater than K_{mc} and similarly K_{md}. Consequently, the increase in the term K_c[P] counterbalances the decreases in the terms K_{mc}[Mc] and K_{md}[Md] in Eq. (22), thus maintaining D_2 relatively constant. When the micelle nucleation mechanism is dominant, D_2 is estimated by

$$D_2 = \delta_m \frac{K_{mc}[\mathrm{Mc}]_0}{k_p \mathrm{M}_w}. \tag{28}$$

where $[\mathrm{Mc}]_0$ is the initial concentration of micelles and δ_m is the parameter introduced to account for the difference between the rates for radical capture by micelles and by particles. The parameter δ_m also includes the effect of the disappearance of micelles to supply emulsifier to those parts of the particle surface produced through particle growth by polymerization.

Equations (5)-(8), (25), (27), and (28) were solved simultaneously. The rate coefficients for free radical capture by particles and micelles, K_c and K_{mc}, respectively, were estimated with a diffusion model, as suggested by Hansen and Ugelstad [27]:

TABLE 1. Constants Used in the Simulation

Monomers	k_p, L/mol·s	$k_{tw} \times 10^{-6}$, L/mol·s	M_w, mol/L	n^*
Styrene (St)	209	115	0.0035	5[a]
Butyl acrylate (BA)	2 100	330	0.011	20[b]
Methyl methacrylate (MMA)	410	24	0.15	66[c]
Vinyl chloride (VCl)	11 000	2 100	0.17	60[b]
Vinyl acetate (VA)	2 640	117	0.29	50[d]
Temperature, °C	50	50	25-50	
Reference	24	24	2	

[a]Hansen and Ugelstad [27].
[b]Assumed in this study.
[c]Fitch and Tsai [19].
[d]Priest [29].

$$K_c = \delta_p 4\pi r_p D_w N_A \tag{29}$$

$$K_{mc} = \delta_{mc} 4\pi r_m D_w N_A \tag{30}$$

where D_w is the diffusion coefficient for free radicals in the aqueous phase; r_p and r_m are the average radii of the particles and micelles, respectively; and N_A is Avogadro's number. The values δ_p and δ_{mc} are introduced to account for radical absorption reversibility by micelles and particles, respectively.

The values used for determining K_c and K_{mc} in the simulation are $D_w = 5 \times 10^{-10}$ dm^2/s, $r_p = 2 \times 10^{-7}$, $r_m = 2 \times 10^{-8}$ dm, and $\delta_p = \delta_{mc} = 1$. The parameter δ_m in Eq. (28) is set equal to 1.0. Other kinetic parameters used are listed in Table 1.

1. Variation of Emulsifier Concentration

Figures 2-6 show the influence of the initial number of micelles present on the number of particles formed, N_s, and on other parameters in the model. In the calculations, ρ_i is 2.2×10^{-8} mol/L·s, and K_f is set equal to 234 L/mol·s.

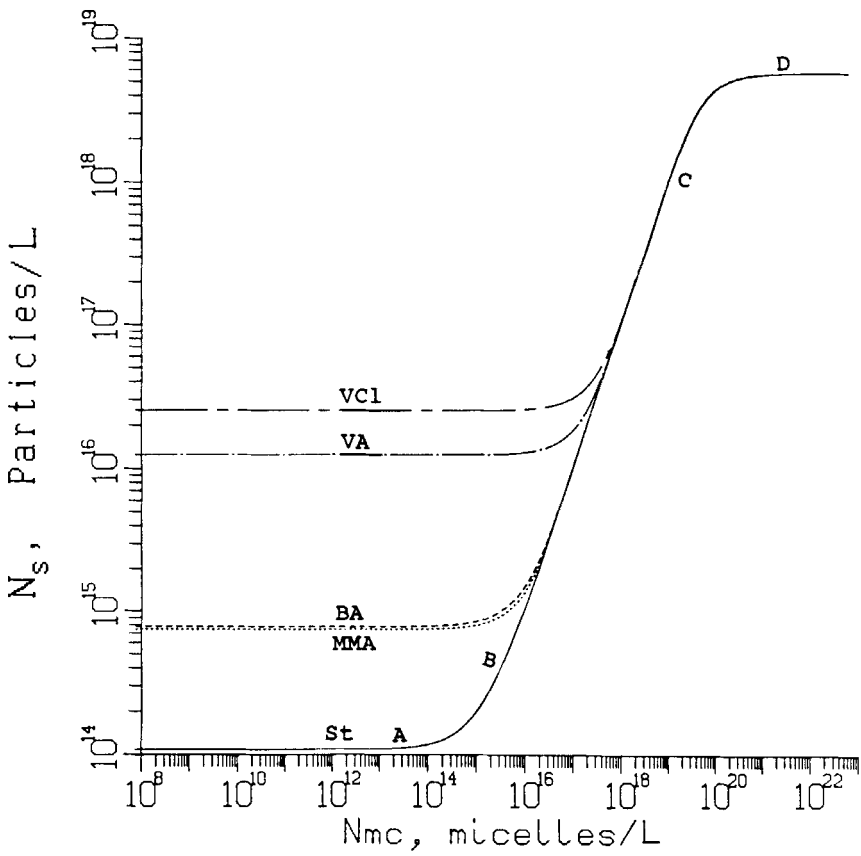

FIG. 2. Variation of the particle number N_s with micelle number N_{mc} for various monomers. $K_f = 234$ L/mol·s, $\rho_i = 2.2 \times 10^{-8}$ mol/L·s.

Figure 2 shows the variation of particle number at the steady state with micelle concentration. Note here that $N_s = N_A [P]_s$. The shape of the N_s vs $[Mc]_0$ curves in Fig. 2 is similar to that in Fig. 1 presented by Vanderhoff [2]. The generally observed S-shaped N_s vs [S] curves, such as shown in Fig. 1, have not yet been simulated by models presented in the literature.

Please note that micelle concentration $[Mc]_0$ is used in Fig. 2 instead of the emulsifier concentration [S]. This implies that the emulsifier concentration is above the critical micelle concentration (CMC). However, the near-horizontal part of the curves at very low $[Mc]_0$ shows that $[Mc]_0$ has little

influence on N_s in this range. In fact, the N_s values of the ordinate are calculated for $[Mc]_0 = 0$ instead of the $[Mc]_0$ value (8×10^8 micelles/L, note $[Mc]_0 = N_{mc}/N_A$ mol/L) indicated at the origin of the log-log coordinates. Thus the near-horizontal part of the curves at low $[Mc]_0$ is due to the domination of homogeneous nucleation, and the values of N_s in this part represent N_s at emulsifier concentrations below the CMC.

Figure 2 shows that N_s in the homogeneous-nucleation-dominated region varies among different monomers. In general, higher polarity favors homogeneous nucleation so that particle concentration is higher for more polar monomers at emulsifier concentrations below the CMC. As the emulsifier concentration increases, the number of micelles in the system is increased, and micelle nucleation begins to compete with homogeneous nucleation. This is shown by the steep rise in N_s at N_{mc} of about 10^{15} micelles/L for styrene, 10^{16} micelles/L for butyl acrylate and methyl methacrylate, 5×10^{17} micelles/L for vinyl acetate, and 10^{18} micelles/L for vinyl chloride. The amount of emulsifier needed to produce such numbers of micelles is small compared to the CMC. Suppose sodium dodecyl sulfate (SDS) is used as the emulsifier for which Vanderhoff [2] reported a CMC of about 0.008 mol/L. If a micelle consists of 60 emulsifier molecules, as suggested by Sutterlin [3], 10^{16} micelles/L requires an emulsifier concentration of only 10^{-6} mol/L, lower than the CMC of 0.008 mol/L.

The small number of micelles just before the steep rise in N_s may be attributed to the aggregation of emulsifier molecules below the CMC, as suggested by Vanderhoff [2]. Vanderhoff, in explaining the steep rise in N_s just below the CMC in Fig. 2, suggested that some of the aggregates of emulsifier might be capable of solubilizing monomer and serving as a locus for particle nucleation. Recent measurements of the partial specific volume of sodium lauryl sulfate solutions by Bonner [20] suggest that aggregates of lauryl sulfate ions are present at concentrations well below the CMC.

Figure 2 also shows that, for the more water-soluble monomers such as VA and VCl, the steep change in N_s occurs at higher N_{mc} than that for sparingly water-soluble monomers such as styrene (St). This is because homogeneous nucleation is more significant for VCl and VA systems so that more micelles are needed for the micelle nucleation mechanism to be able to compete with homogeneous nucleation. The contribution of various reaction mechanisms to the steady-state particle concentration can be illustrated by the other parameters of the model.

Figure 3 shows the variation with $[Mc]_0$ of α_p which represents the probability of free-radical propagation in the aqueous phase. A radical needs to add $n^* - 1$ monomeric units before it precipitates from the aqueous phase by

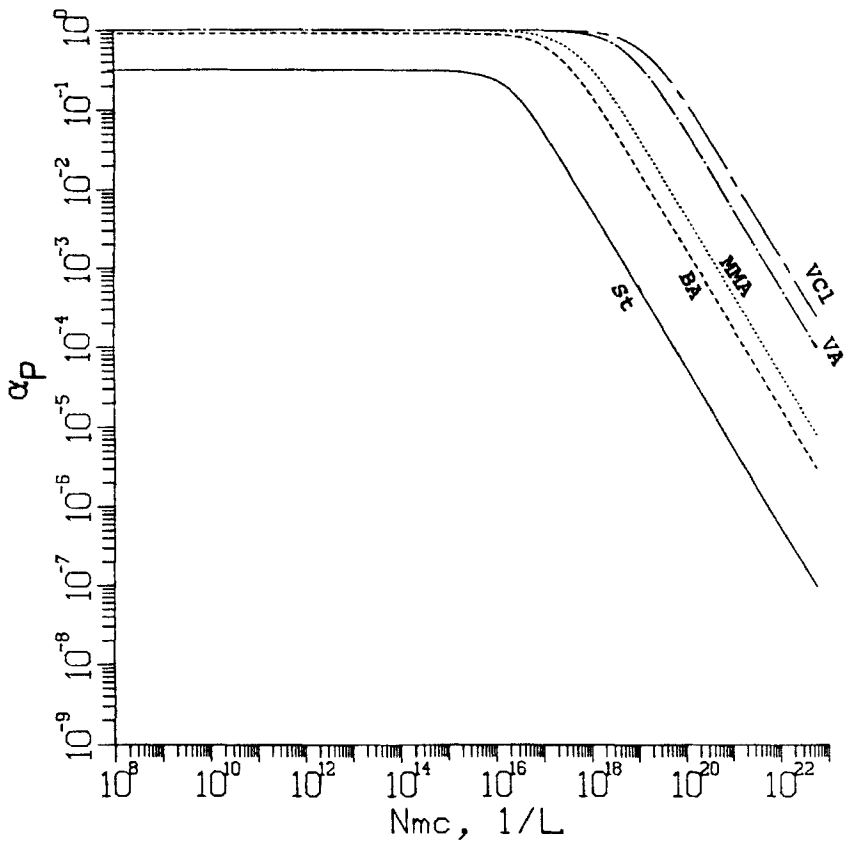

FIG. 3. Variation of the aqueous-phase propagation probability α_p with micelle number N_{mc} for various monomers. K_f = 234 L/mol·s, $\rho_i = 2.2 \times 10^{-8}$ mol/L·s.

homogeneous nucleation. Thus, the probability of homogeneous nucleation will be $\alpha_p^{n^*-1}$. Large α_p values favor homogeneous nucleation. Figure 3 shows that α_p is small for nonpolar monomers such as St. As the micelle concentration increases, micelles will compete with monomer molecules in the aqueous phase to capture radicals so that α_p decreases. The concentration of micelles at which α_p begins to drop corresponds to the point at which N_s begins to rise in Fig. 2. This concentration increases with increasing water solubility of the monomer.

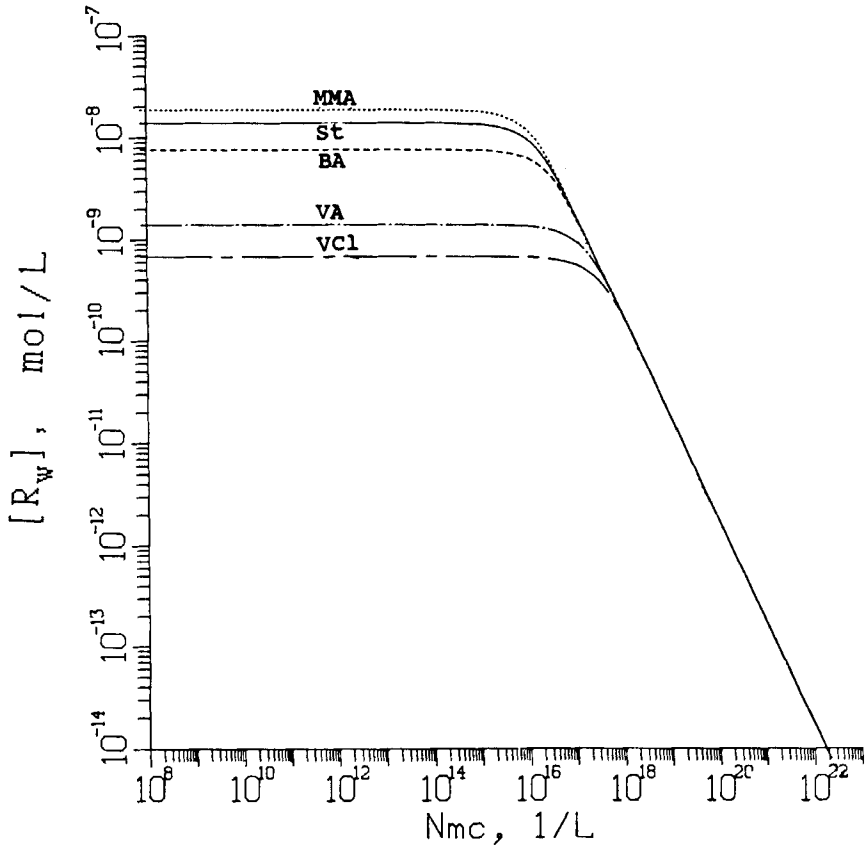

FIG. 4. Variation of the total radical concentration in the aqueous phase $[R_w]$ with micelle number N_{mc} for various monomers. $K_f = 234$ L/mol·s, $\rho_i = 2.2 \times 10^{-8}$ mol/L·s.

The point at which micelles begin to contribute to particle nucleation can also be illustrated by the decrease in the total radical concentration in the aqueous phase, $[R_w]$, with increasing micelle concentration, as shown in Fig. 4. Figure 5 shows the variation of b with $[Mc]_0$. The parameter b in our model, and also suggested by Fitch and Tsai [19], accounts for aqueous-phase termination. It is always less than unity, as seen from its definition (Eq. 7). Smaller b values reflect more significant aqueous-phase termination. Figure 5

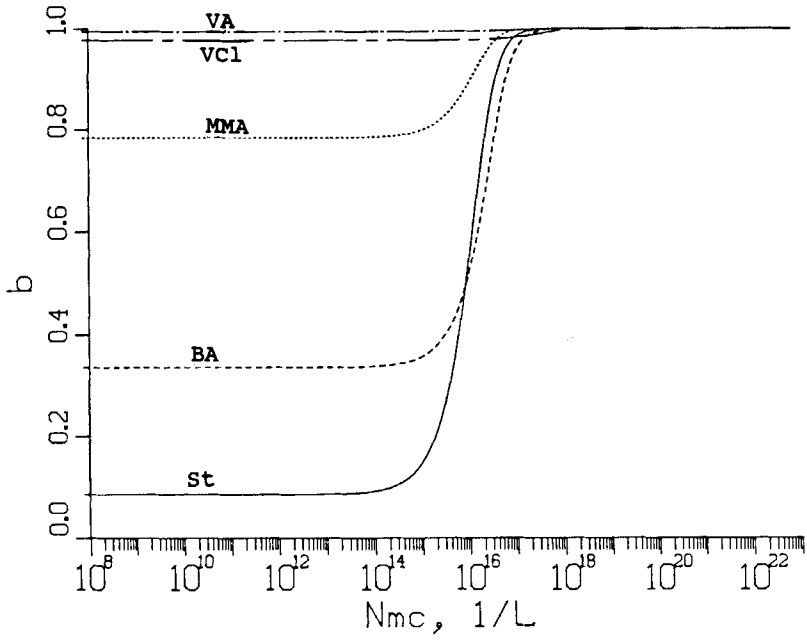

FIG. 5. Variation of b with micelle number N_{mc} for various monomers. $K_f = 234$ L/mol·s, $\rho_i = 2.2 \times 10^{-8}$ mol/L·s.

shows that b decreases with decreasing water solubility of the monomers at emulsifier concentrations below the CMC. At emulsifier concentrations far above the CMC, large numbers of micelles will capture almost all radicals and prevent aqueous-phase termination. Therefore, b tends to be 1.0, no matter what monomers are used.

Figure 6 shows the variation of C with N_{mc}. C is the fraction of dead oligomers produced by aqueous-phase termination that have chain lengths exceeding n^*. These oligomers will precipitate from the aqueous phase to form new particles. Similar to b in Fig. 5, C in Fig. 6 increases with increasing water solubility of the monomer at emulsifier concentrations below the CMC. Aqueous-phase termination is extremely limited at emulsifier concentrations far above the CMC. As a result, C tends to be zero.

Figure 2 shows that all curves converge above that 10^{18} micelles/L, because the same value (234 L/mol·s) of the particle coagulation coefficient K_f is used for all monomer systems. However, in practice, K_f would be expected

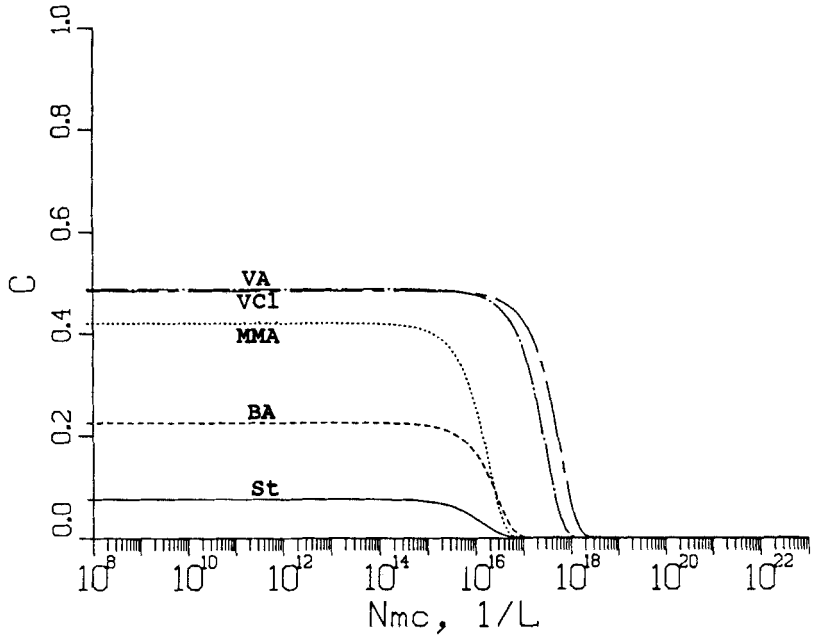

FIG. 6. Variation of C with micelle number N_{mc} for various monomers. $K_f = 234$ L/mol•s, $\rho_i = 2.2 \times 10^{-8}$ mol/L•s.

to vary among different monomer systems. Sutterlin [3] suggested that the more hydrophobic monomers presented a reduced agglomeration tendency. Therefore, K_f should decrease with decreasing polarity of the monomer. The influence of K_f on the shape of N_s vs $[\mathrm{Mc}]_0$ curves is shown in Figs. 7-11 for different values of K_f for each monomer. The slope of the log N_s vs log $[\mathrm{Mc}]_0$ curves at emulsifier concentrations well above the CMC decreases as K_f increases. Thus, if smaller values of K_f are assumed for less polar monomers, the slope of these curves would be expected to decrease with increasing monomer polarity. Such results are consistent with the experimental facts reported by Sutterlin [3]. In fact, all the features observed by Sutterlin [3] for N_s vs [S] curves in the three regions, which were discussed earlier, appear in Fig. 2 and Figs. 7-11, obtained by computer simulation with the new model.

The near-horizontal part of the log N_s vs log $[\mathrm{Mc}]_0$ curves at emulsifier concentrations well above the CMC suggests that, here, N_s is determined

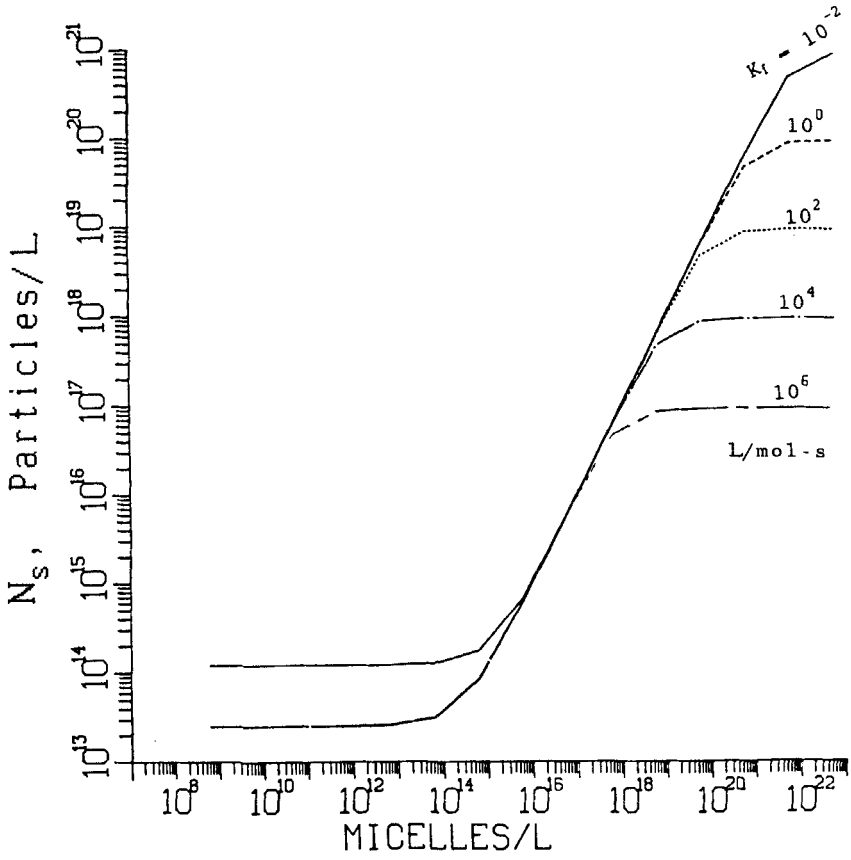

FIG. 7. Variation of the particle number N_s with micelle number N_{mc} for styrene at different values of the coagulation rate constant K_f. $\rho_i = 2.2 \times 10^{-8}$ mol/L·s.

more by the rate of radical generation than by the number of micelles. That is, the availability of radicals to enter micelles for particle nucleation becomes the controlling step. Particle coagulation can also contribute to this near-horizontal part of the $\log N_s$ vs $\log [\mathrm{Mc}]_0$ curves. As $[\mathrm{Mc}]_0$ increases, N_s increases. Consequently, the extent of particle coagulation will increase, as indicated by the last term in Eq. (2). Eventually, an equilibrium will be reached when the increase in N_s due to increasing $[\mathrm{Mc}]_0$ is just compensated for by the de-

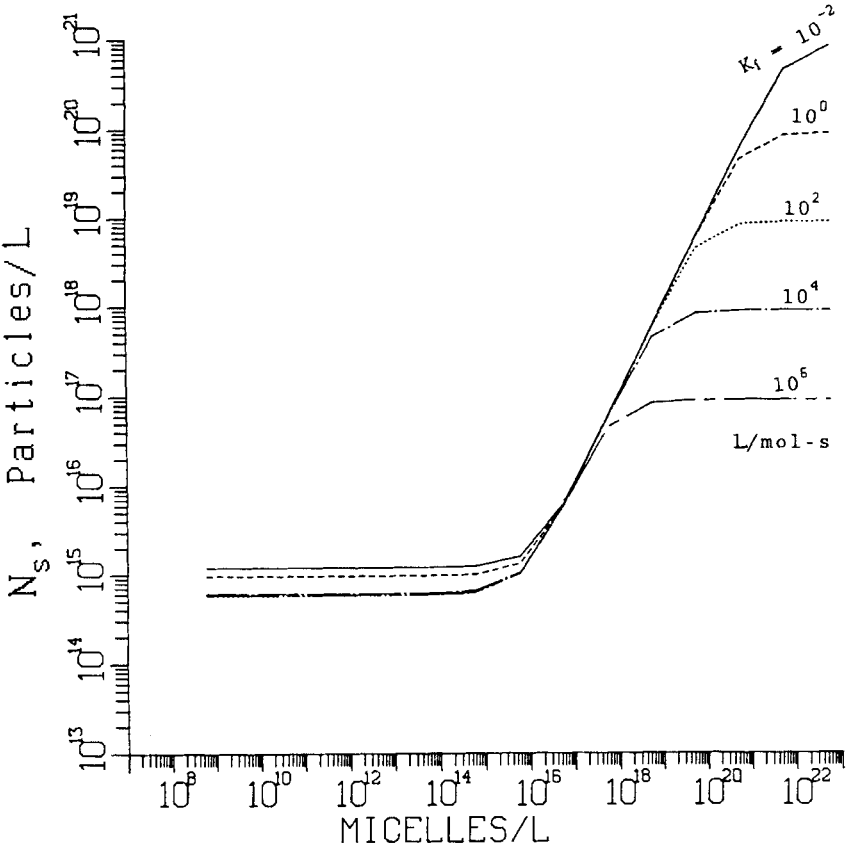

FIG. 8. Variation of the particle number N_s with micelle number N_{mc} for butyl acrylate at different values of the coagulation rate constant K_f. $\rho_i = 2.2 \times 10^{-8}$ mol/L·s.

crease in N_s due to increased coagulation, thus causing N_s to be independent of $[Mc]_0$.

Significant literature exists concerning the dependence of particle concentration on initiator and emulsifier concentrations. Thus, a more detailed discussion of emulsifier concentration effects seem appropriate. Figure 2 shows that the slope of the log N_s vs log $[Mc]_0$ curve changes with emulsifier concentration. At very low emulsifier concentration where the homogeneous

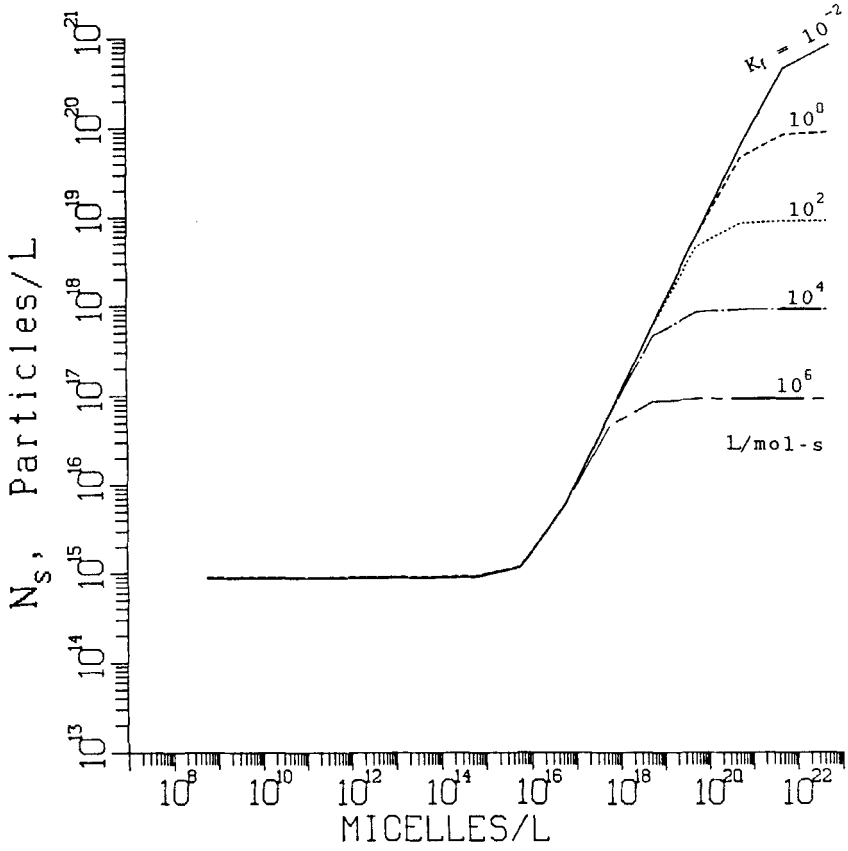

FIG. 9. Variation of the particle number N_s with micelle number N_{mc} for methyl methacrylate at different values of the coagulation rate constant K_f. $\rho_i = 2.2 \times 10^{-8}$ mol/L·s.

nucleation mechanism dominates, the slope is close to zero. The slope is about 1.0 in the range of emulsifier concentration where particle concentration increases steeply with increasing $[Mc]_0$ (section BC in Fig. 2). Emulsifier concentrations usually employed in emulsion polymerization are located within the section CD of Fig. 2, where the slope changes from 1.0 to almost zero. This is why the exponents of emulsifier concentration reported in the literature are so widely scattered. It should also be noted that the ranges of emulsi-

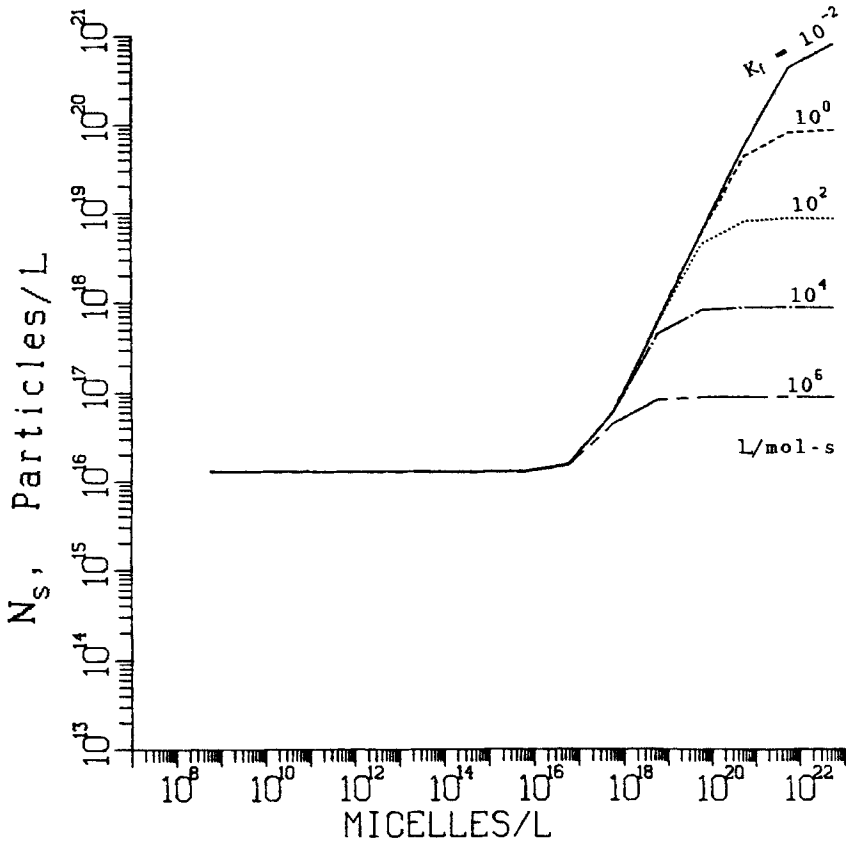

FIG. 10. Variation of the particle number N_s with micelle number N_{mc} for vinyl acetate at different values of the coagulation rate constant K_f. $\rho_i = 2.2 \times 10^{-8}$ mol/L·s.

fier concentration investigated in the literature are narrow (less than two orders of magnitude), and, moreover, these experiments were generally designed for comparison with the Smith-Ewart theory which predicts a power relationship between N_s and [S]. As a result, straight lines were likely to result on the log N_s vs log [S] plots of these investigations. However, studies by Sutterlin [3], Okamura and Motoyama [21], and Van der Hoff [22] which involve a large range of emulsifier concentrations yielded sigmoidal curves like

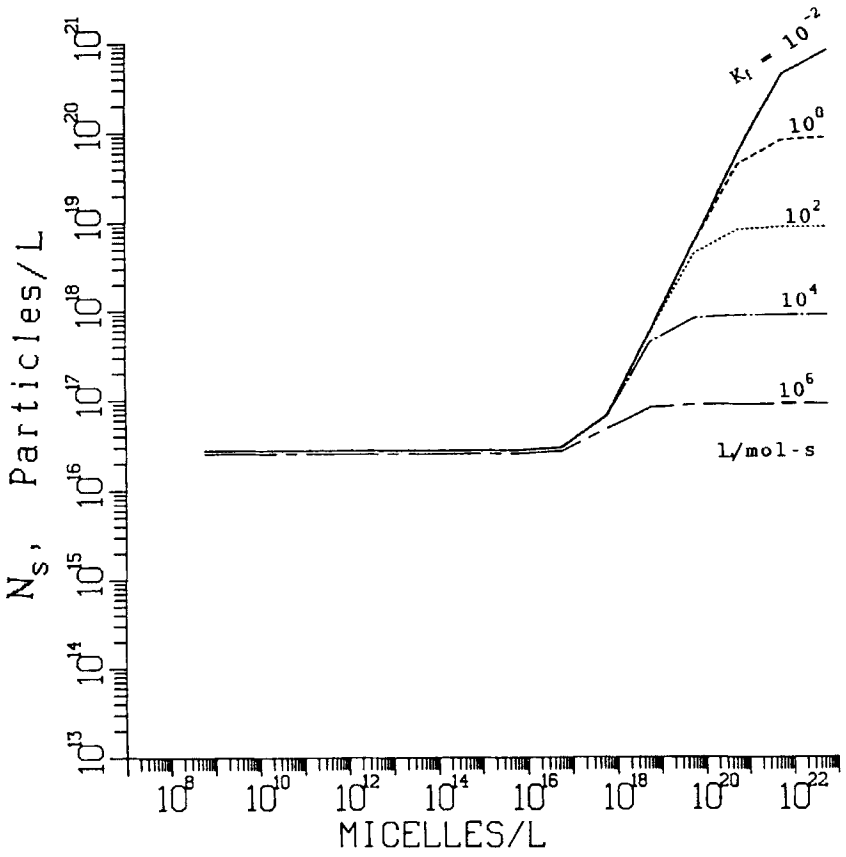

FIG. 11. Variation of the particle number N_s with micelle number N_{mc} for vinyl chloride at different values of the coagulation rate constant K_f. $\rho_i = 2.2 \times 10^{-8}$ mol/L·s.

that presented by Vanderhoff [2] in Fig. 1 and predicted by our model in Fig. 2. Therefore, when discussing the relationship between emulsifier concentration and particle number, the reaction conditions must be specified.

2. Variation of Initiation Rate

Variation of the rate of initiation of radicals in the aqueous phase also influences the shape of $\log N_s$ vs $\log [Mc]_0$ curves (Figs. 12-16). When emul-

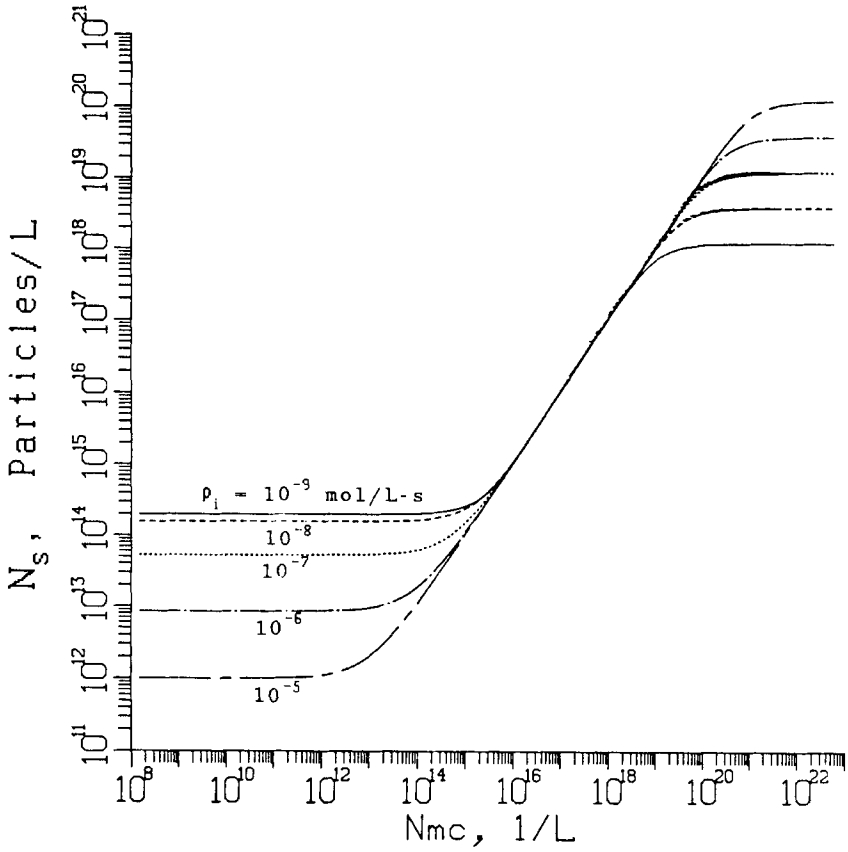

FIG. 12. Variation of the particle number N_s with micelle number N_{mc} for styrene at different values of the initiation rate ρ_i. $K_f = 234$ L/mol·s.

sifier concentrations are above the CMC, the particle concentration increases with increasing initiation rate. The slopes of these curves for all monomers decrease with decreasing radical initiation rate at emulsifier concentration just above the CMC. The slopes tend to be zero and independent of initiation rate as the emulsifier concentration increases far beyond the CMC.

When low micelle concentrations are used, the homogeneous nucleation mechanism dominates and the initiation rate has a different influence on the various monomer systems. Figures 12-16 show that the particle concentra-

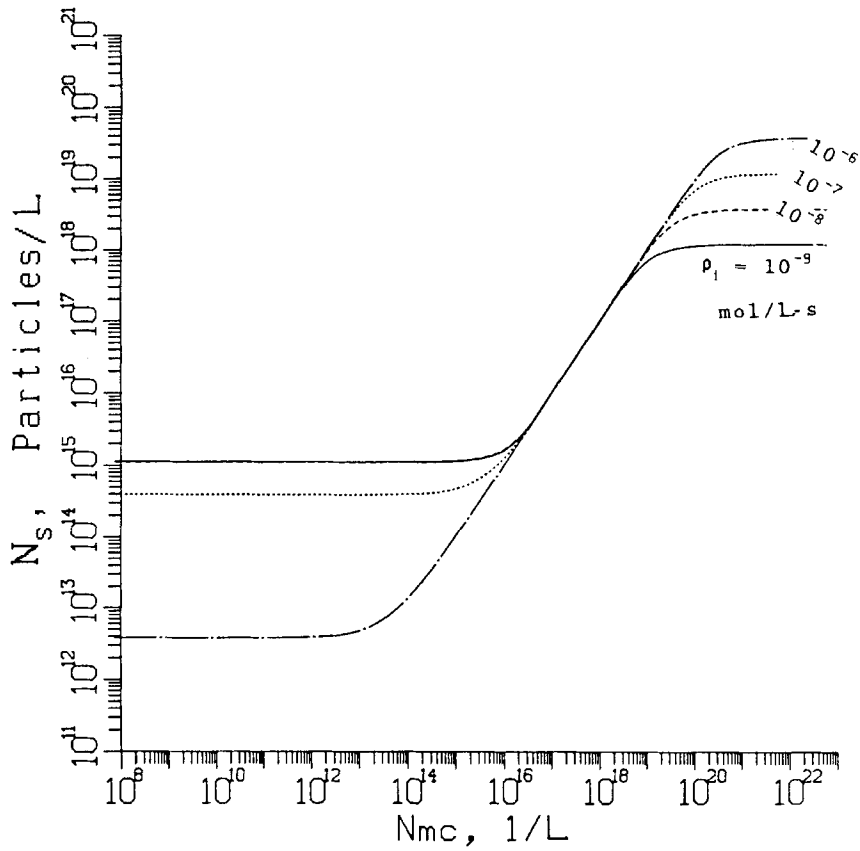

FIG. 13. Variation of the particle number N_s with micelle number N_{mc} for butyl acrylate at different values of the initiation rate ρ_i. K_f = 234 L/mol·s.

tion decreases with increasing initiation rate. This prediction, however, does not reflect the real situations, considering that the same K_f (234 L/mol·s) was used for all the initiation rates in the simulation. The low emulsifier concentration region in Figs. 12-16 can be considered as an emulsifier-free region. In emulsifier-free systems, particles are stabilized, in most cases, by initiator end groups. Obviously, any change in the initiation rate by increasing initiator concentration will increase the number of initiator end groups for stabilizing particles, resulting in a decrease of K_f. It has been shown above that N_s in-

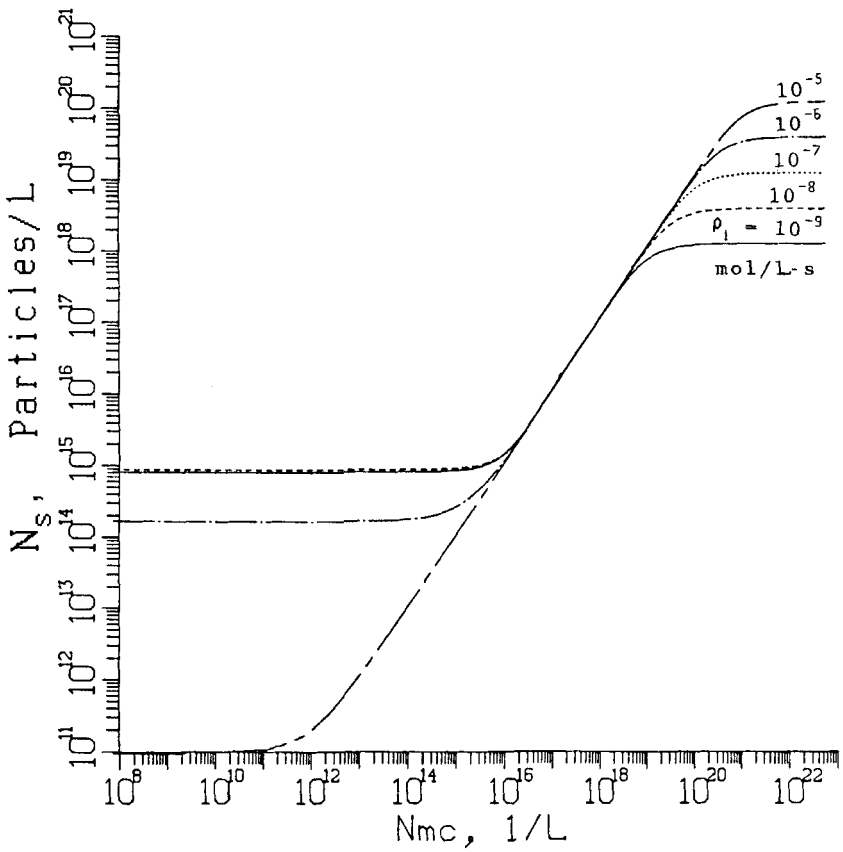

FIG. 14. Variation of the particle number N_s with micelle number N_{mc} for methyl methacrylate at different values of the initiation rate ρ_i. K_f = 234 L/mol·s.

creases as K_f decreases. If K_f decreases as the initiation rate increases, N_s may increase with increasing initiation rate instead of the opposite as indicated in the low N_{mc} region in Figs. 12-16. In contrast, a constant value of K_f assumed for different initiation rates in the high emulsifier concentration region, which we discussed above, is reasonable since now particles are stabilized mainly by emulsifier molecules, and N_s is compared at the same emulsifier concentration. Therefore, the predictions by Figs. 12-16 at high emulsifier concentration reflect real situations.

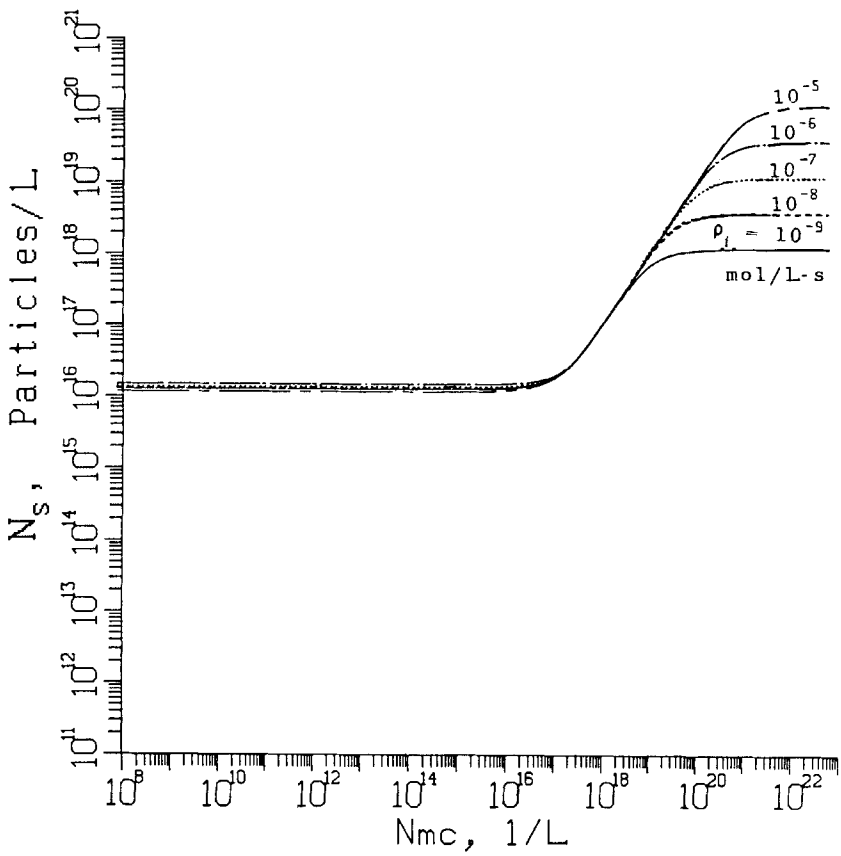

FIG. 15. Variation of the particle number N_s with micelle number N_{mc} for vinyl acetate at different values of the initiation rate ρ_i. $K_f = 234$ L/mol·s.

Figures 17-19 show the influence of ρ_i on α_p, $[R_w]$, and b. ρ_i has little influence on α_p and b at high micelle concentration. This is expected since free-radical absorption by micelles is much more significant than radical propagation and termination in the aqueous phase. At low micelle concentrations, however, both α_p and b decrease with increasing ρ_i. This results from the increasing termination in competition with the propagation reaction in the aqueous phase because of the increased free-radical concentration in the aqueous phase, $[R_w]$. The increase in $[R_w]$ with increasing ρ_i

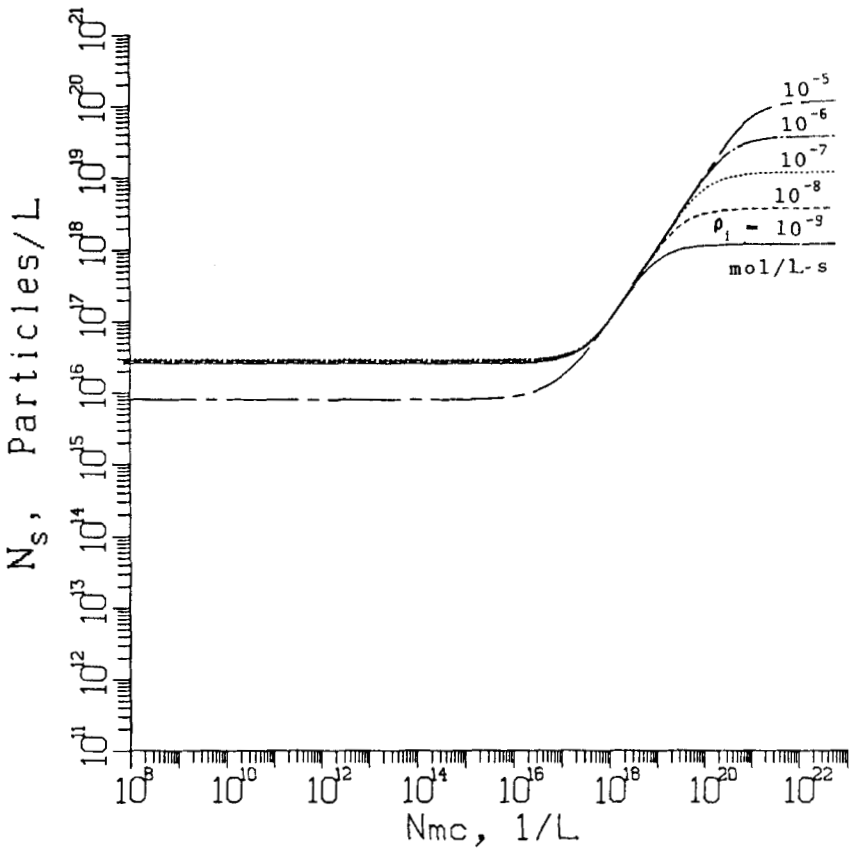

FIG. 16. Variation of the particle number N_s with micelle number N_{mc} for vinyl chloride at different values of the initiation rate ρ_i. $K_f = 234$ L/mol·s.

is demonstrated by Fig. 18. Initiation rates affect $[R_w]$ over the whole range of micelle concentration.

The effect of ρ_i on the final particle number N_s can be better shown by plotting N_s against ρ_i at fixed emulsifier concentration while changing K_f, as shown in Figs. 20-22. At emulsifier concentrations above CMC, N_s increases with increasing ρ_i until it reaches a constant value at high ρ_i. The slope of the straight line in the increasing region is about 0.5, in agreement with the

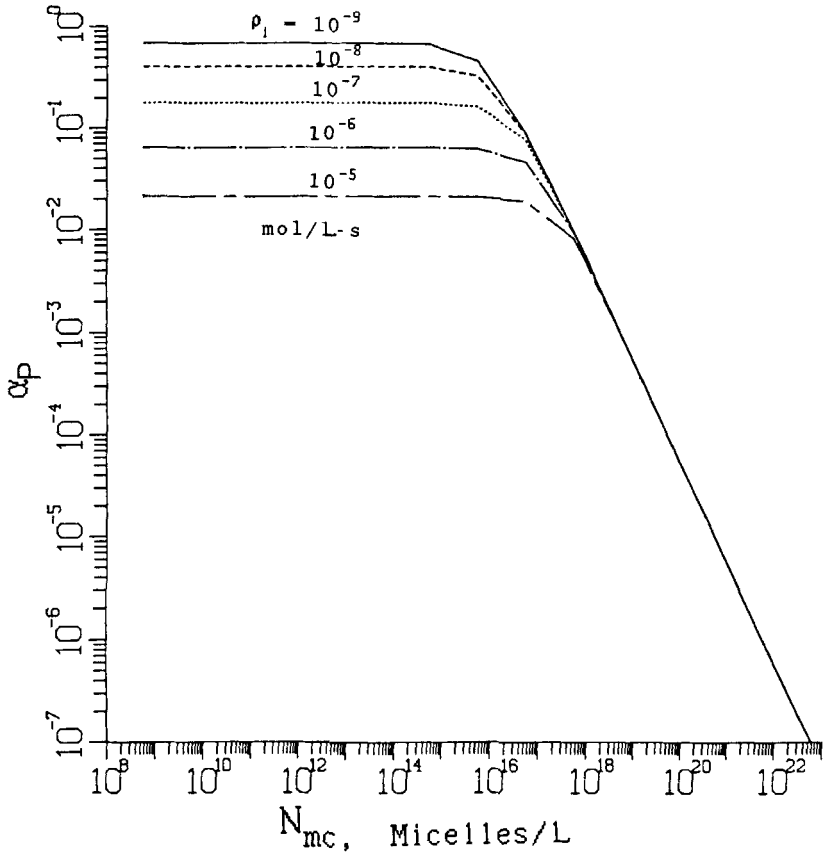

FIG. 17. Variation of α_p with micelle number N_{mc} for styrene at different values of the initiation rate ρ_i. $K_f = 234$ L/mol·s.

prediction of the Medvedev model [23], which assumes initiation on the micelle surface and is close to the 0.4 power dependence of N_s on [S] predicted by the Smith-Ewart theory. As ρ_i increases, the slope of the log N_s vs log ρ_i curve decreases. At very high ρ_i, N_s becomes independent of ρ_i. Here, the value of N_s is determined more by the number of micelles produced and by aqueous-phase termination than by the rate of radical generation. That is, the fixed number of micelles and increased aqueous phase termination due to increased radical concentration limit and control the particle formation.

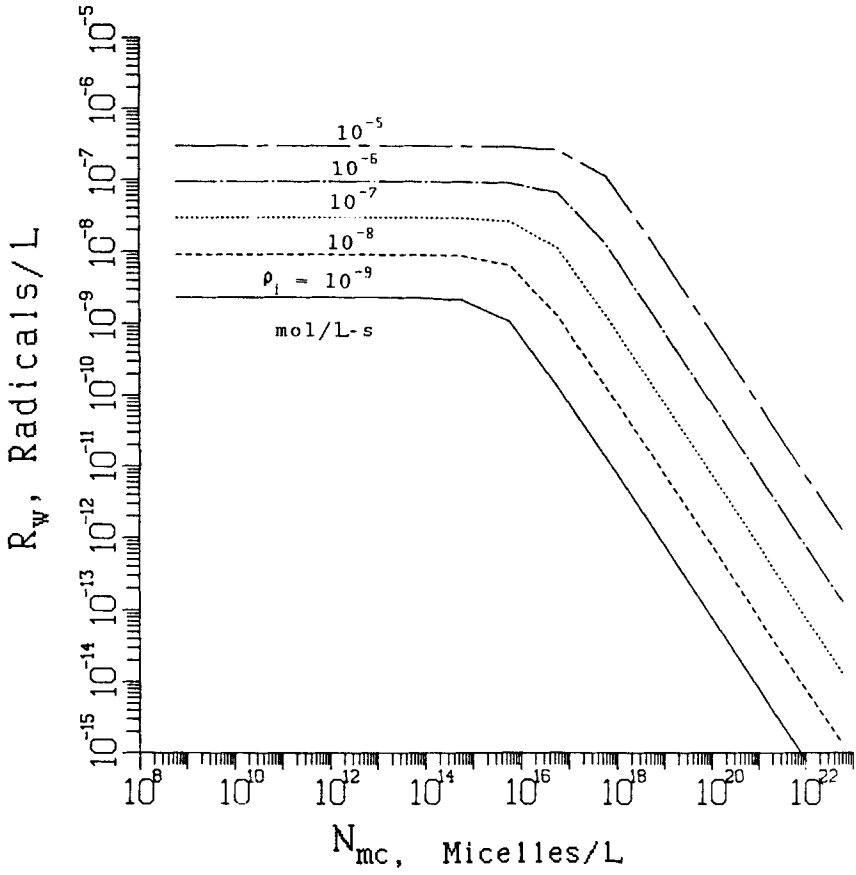

FIG. 18. Variation of the total radical concentration in the aqueous phase R_w with micelle number N_{mc} for styrene at different values of the initiation rate ρ_i. $K_f = 234$ L/mol·s.

Figures 20-22 also show that a greater tendency for particle coagulation (i.e., larger K_f) causes N_s to tend to a constant value at a higher ρ_i. The systems with larger K_f have smaller N_s before rising to the constant level for the fixed value of ρ_i.

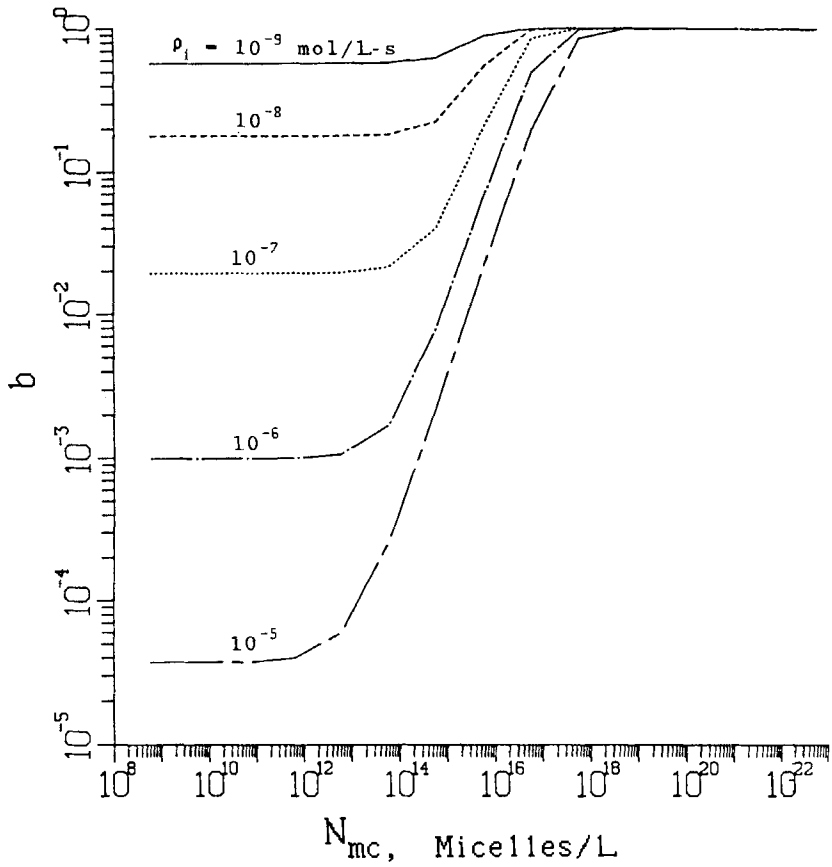

FIG. 19. Variation of b with micelle number N_{mc} for styrene at different values of the initiation rate ρ_i. $K_f = 234$ L/mol·s.

3. Some Limiting Cases of the Model

The particle number at the steady state is determined by

$$N_s = \frac{N_A \rho_i K_c B B_i}{2K_f} \left\{ \sqrt{1 + \frac{4bK_f}{\rho_i (K_c B B_i)^2}} - 1 \right\}. \tag{24}$$

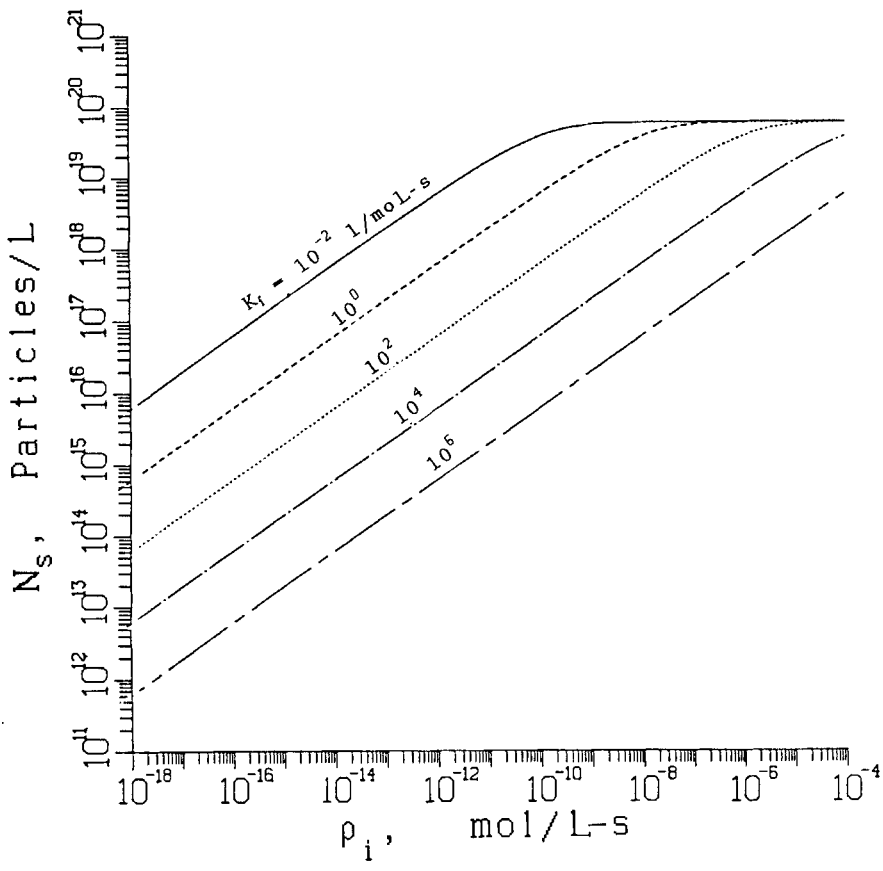

FIG. 20. Variation of the particle number N_s with initiation rate ρ_i for styrene at different values of the coagulation rate constant K_f. $N_{mc} = 6.023 \times 10^{20}$ micelles/L.

(a) When $B_4 = 4bK_f/[\rho_i(K_cBB_i)^2]$ is much less than 1, $(1 + B_4)^{1/2} \cong 1 + (B_4/2)$ and Eq. (24) reduces to

$$N_s = bN_A/(K_cBB_i). \tag{31}$$

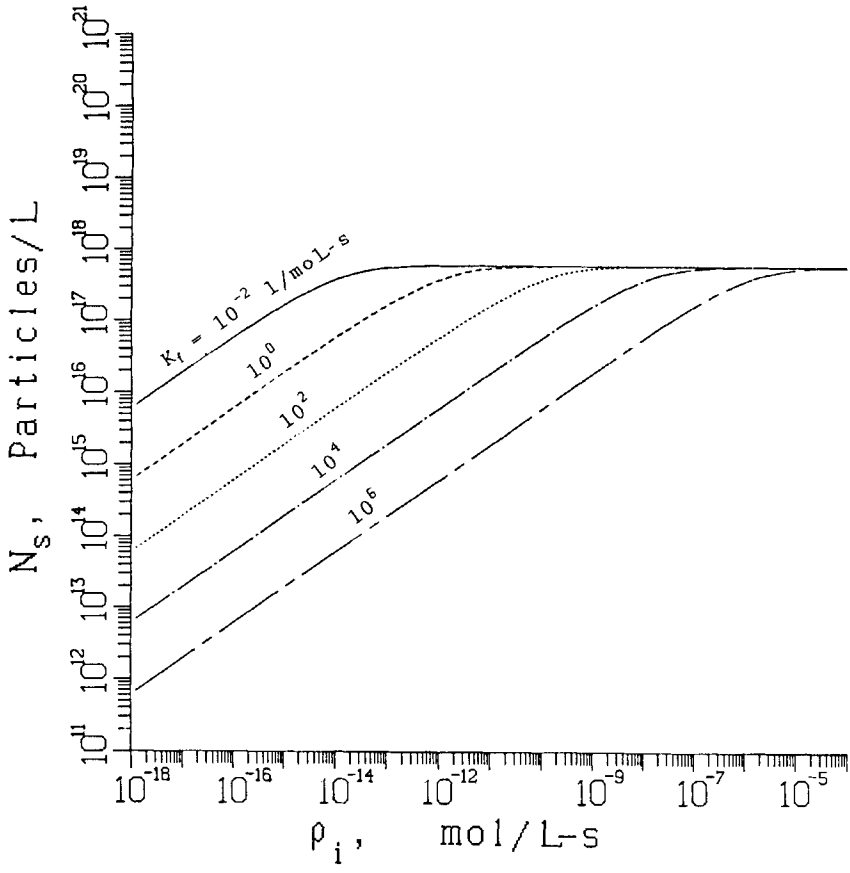

FIG. 21. Variation of the particle number N_s with initiation rate ρ_i for styrene at different values of the coagulation rate constant K_f. $N_{mc} = 6.023 \times 10^{18}$ micelles/L.

Assuming $B_i = 1$ and substituting Eq. (5) into Eq. (31) gives

$$N_s = \frac{N_A k_p M_w b(1 - \alpha_p)}{K_c \alpha_p (1 - \alpha_p{}^{n^*-1})} \tag{32}$$

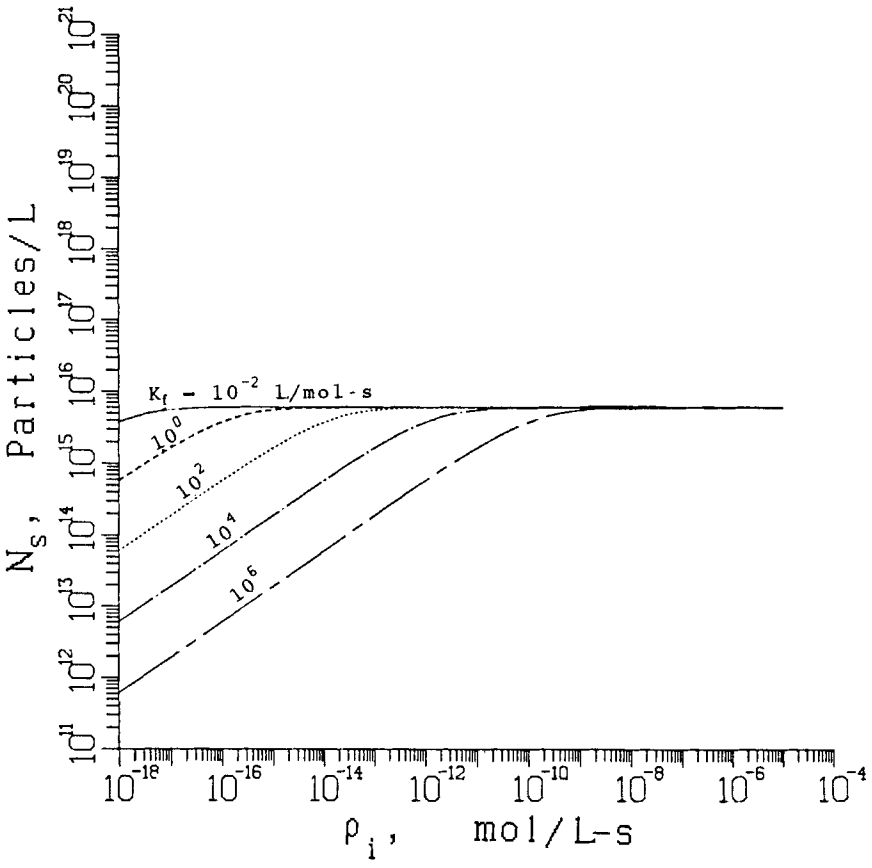

FIG. 22. Variation of the particle number N_s with initiation rate ρ_i for styrene at different values of the coagulation rate constant K_f. N_{mc} = 6.023 × 10^{16} micelles/L.

When α_p is small so that $\alpha_p{}^{n^*-1}$ can be neglected, D_2 can be calculated by Eq. (26). When $[\mathrm{Mc}]_0 = 0$ and monomer of low water solubility is used (Fig. 3), $D_2 = 0$ and the following equation can be used for estimating α_p:

$$\alpha_p = \sqrt{D_1}/(\sqrt{D_1} + D_1). \tag{33}$$

Substituting Eqs. (27) and (33) into Eq. (31) yields

$$N_s \cong N_A b k_{tw}^{1/2} \rho_i^{1/2} / K_c. \tag{34}$$

At low initiator concentration, $b = 1$ (Fig. 19), and the above equation suggests that N_s is proportional to the 0.5 power of ρ_i, as shown in Fig. 20. The slope of the straight part of the $\log N_s$ vs $\log \rho_i$ plot is about 0.5.

(b) When $B_4 >> 1.0$, $(1 + B_4)^{1/2} - 1) \cong B_4^{1/2}$. Equation (24) can be reduced to

$$N_s = N_A b^{1/2} \rho_i^{1/2} / K_f^{1/2}. \tag{35}$$

Equation (35) indicates the 0.5 power dependence of N_s on ρ_i when $b = 1$, i.e., when the emulsifier concentration is far above the CMC or when a more water-soluble monomer is used (Fig. 5) or when ρ_i is very low (Fig. 19).

(c) When $K_f = 0$, N_s can be obtained directly from Eq. (2) by setting $d[\mathrm{P}]/dt = 0$. Thus,

$$N_s = \frac{N_A b \rho_i}{K_c B B_i} = \frac{N_A b k_p \mathrm{M}_w (1 - \alpha_p)}{K_c B_i \alpha_p (1 - \alpha_p{}^{n^*-1})}. \tag{36}$$

When α_p is small (this condition can be met when $[\mathrm{Mc}]_0$ is large, as shown in Fig. 3), $\alpha_p{}^{n^*-1}$ can be neglected and Eq. (26) can be used. If $[\mathrm{Mc}]_0$ is high so that $D_2 >> D_1$, Eq. (26) reduces to [by using $(1 + x)^{1/2} \approx 1 + (x/2)$]:

$$\alpha_p = 1/(1 + D_2). \tag{37}$$

Substituting Eq. (37) into Eq. (36) and rearranging yields

$$N_s = N_A b K_{mc} [\mathrm{Mc}]_0 / K_c. \tag{38}$$

Because $[\mathrm{Mc}]_0$ is high, $b = 1$ (Fig. 5). Therefore, Eq. (38) indicates that N_s depends on $[\mathrm{Mc}]_0$ to the first power when particle coagulation is negligible. This can be shown by the slope of the $\log N_s$ vs $\log [\mathrm{Mc}]_0$ curves in Figs. 7-11 at very high $[\mathrm{Mc}]_0$ for K_f near zero.

COMPARISON WITH EXPERIMENTAL DATA

Experimental data have been taken from Sutterlin [3] who investigated the polymerization of styrene and a series of methacrylates and acrylates over a wide range of emulsifier concentrations. The reaction conditions were as follows: 630 g water, 160 g monomer, and variable amounts of sodium lauryl sulfate (SLS) were emulsified and heated to 82°C in a 2-L reactor equipped with a stirrer and contact thermometer. The polymerization was started with a solution of $(NH_4)_2S_2O_8$ initiator in 10 g water. As a result of the initiator addition, the temperature dropped to 80°C, and this temperature was maintained during the polymerization. Methyl acrylate polymerization was carried out at 73°C because of the low boiling point of the monomer. Particle numbers were determined after complete conversion by turbidity measurements, correlated with electron microscopy and light-scattering measurements.

The kinetic parameters used in the model simulations are listed in Table 2. The propagation rate constant, k_p, and the termination rate constant, k_{tw}, for styrene are calculated from the following equations, which are obtained by regression of the data presented by Brandrup and Immergut [24] with the Arrhenius equation.

$$k_p = 1.052 \times 10^9 \exp(-5052.3/T), \tag{39}$$

$$k_{tw} = 4.0225 \times 10^{13} \exp(-4302/T). \tag{40}$$

Values of $k_p = 22$ and $k_{tw} = 18\,000$ L/mol·s for butyl acrylate (BA) at 80°C were obtained by extrapolation with the Arrhenius equation from the data at 25 and 35°C of Brandrup and Immergut [24]. Values of $k_p = 3155$ and $k_{tw} = 1.015 \times 10^7$ L/mol·s for methyl acrylate (MA) were calculated from the following equations, given by Flory [25] and Goodall and Wilkinson [26]:

$$k_p = 10^8 \exp(-3586/T), \tag{41}$$

$$k_{tw} = 1.5 \times 10^{10} \exp(-2525/T). \tag{42}$$

The decomposition rate constants k_d for $(NH_4)_2S_2O_8$ were taken from the data for $K_2S_2O_8$ of Brandrup and Immergut [24]. Values of k_d at 73°C were obtained by interpolation. The initiator efficiency f is assumed to be 0.3 for all conditions. Values of f between 0.3 and 0.4 have been reported by Van der Hoff [22] for $K_2S_2O_8$ in a styrene system. In determining K_c

TABLE 2. Kinetic Parameters Used in the Model Simulation of Sutterlin's Experiments [3]

Monomer		St	BA	MA	Ref.
Temperature	°C	80	80	73	
[S]	mol/L	Variable	Variable	Variable	
[I] $\times 10^3$	mol/L	Variable	6.35	6.35	
$K_d \times 10^5$	s^{-1}	9.16	9.16[a]	3.19[a]	24
k_p	L/mol·s	640	22[a]	3155	24, 30, 25
$k_{tw} \times 10^{-6}$	L/mol·s	205	0.018	10.15	24, 30, 25
M_w	mol/l	0.0035	0.011	0.65	3
n^*		5	20[b]	80[b]	26
f		0.3	0.3	0.3	22
r_p	Å	672	672	672	
r_m	Å	12.6	12.6	12.6	28
$D_w \times 10^{10}$	dm^2/s	5.0	5.0	5.0	27
K_f	L/mol·s	750	750	2500	
δ_m		Varies with [I]			

[a]Obtained by interpolation or extrapolation of the data of Brandrup and Immergut [24].

[b]Assumed in this study.

and K_{cm} by Eqs. (29) and (30), the micelle radius r_m and particle radius r_p are assumed to be 12.6 and 673 Å, respectively. The diffusion coefficient for radicals in water, D_w, is assumed to be 5×10^{-10} dm^2/s, as given by Hansen and Ugelstad [27]. The monomer concentration in the aqueous phase, M_w, is approximated by the solubility of the monomer in water. Thus M_w = 0.0035, 0.011, and 0.65, as reported by Vanderhoff [2], are used for styrene, butyl acrylate, and methyl acrylate, respectively. A critical chain length for homogeneous nucleation, n^*, of 5 for styrene was recommended by Goodall and

Wilkinson [26]. For methyl methacrylate, n^* has been determined by Fitch and Tsai [19] to be about 66. Considering the difference in their water solubilities, values of 20 and 80 for n^* are assumed for BA and MA, respectively.

The initial micelle concentration $[Mc]_0$ is determined by

$$[Mc]_0 = ([S] - CMC)/mc, \tag{43}$$

where [S] is the emulsifier concentration charged, mc is the number of emulsifier molecules in a micelle and is taken to be 60 in the model calculation, as recommended by Odian [28], and CMC is the critical micelle concentration. The CMC for sodium lauryl sulfate (SLS) measured by physical means (such as changes in surface tension and electrical conductivity) is reported by Sutterlin [3] to be 6.35×10^{-3} mol/L. The CMC measured physically, however, does not really correspond to the critical point at which micelles are formed for particle nucleation. Vanderhoff [2] reported that aggregates of SLS are present at concentrations well below the physically measured CMC. These aggregates of the surfactant molecules are obviously able to serve as sites for particle nucleation. Therefore, in the model simulation, 10^{-5} mol/L is assumed for the CMC in Eq. (43).

The average particle coagulation rate coefficient K_f is set equal to 750 L/mol·s for both styrene and butyl acrylate. According to Sutterlin [3], particle coagulation is more significant with more water-soluble monomer systems. Therefore, a K_f of 2500 L/mol·s is assumed for methyl acrylate. In fact, K_f was used as an adjustable parameter in the model simulation, and these values of K_f were obtained by fitting the experimental data.

The parameter δ_m in Eq. (28) was found to change with initiator concentration [I], and the following equation was used:

$$\delta_m = 0.2296 + 2.138[I]^{0.5}. \tag{44}$$

This gives $\delta_m = 0.4$ for styrene, butyl acrylate, and methyl acrylate for [I] = 6.35×10^{-3} mol/l.

Comparison of experimental results with model simulations are shown in Figs. 23-30; the symbols are experimental data and the lines are model predictions. The theoretical predictions are generally in agreement with the experimental data. The poor agreement at low emulsifier concentration in Figs. 23-29 probably results from the use of Eq. (28) for calculating D_2. Equation (28) is derived based on the assumption of domination by the micelle nucleation mechanism, which is obviously not very good at low emulsifier concentrations. In addition, the same initiator efficiency, $f = 0.3$, has been assumed

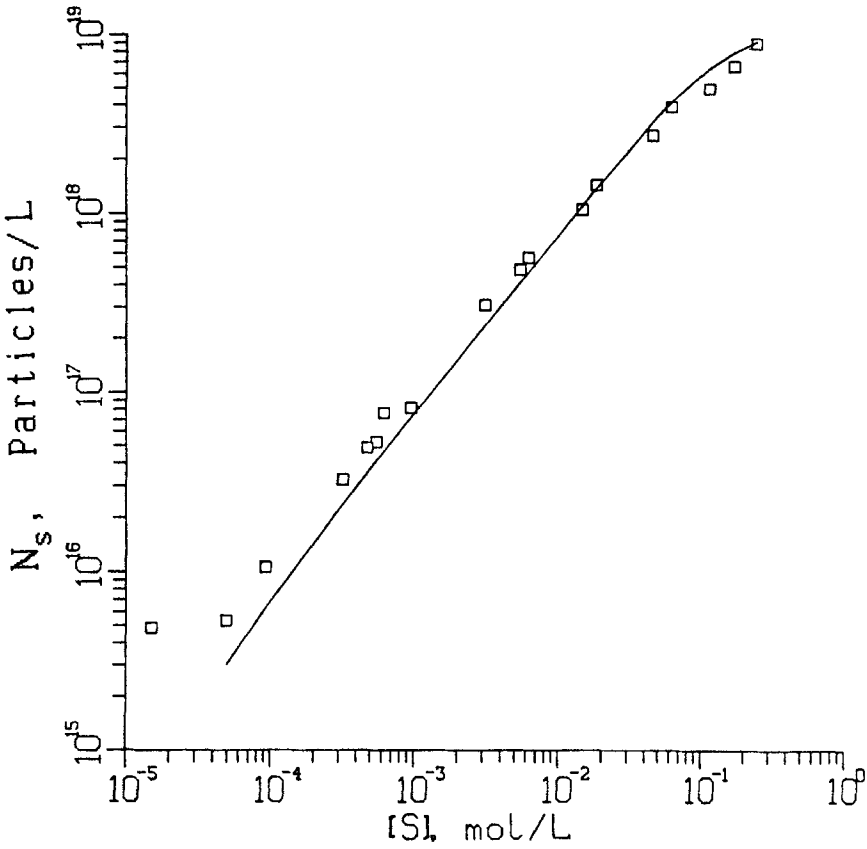

FIG. 23. Variation of the particle number N_s with emulsifier concentration [S] for butyl acrylate at 80°C. Initiator ($(NH_4)_2S_2O_8$), [I] = 0.00635 mol/L. Symbols are experimental data [3]. Curve is from the model prediction with K_f = 750 L/mol·s, f = 0.3, δ_m = 0.4.

for all systems even though a wide range of emulsifier concentrations was investigated (about 4 orders of magnitude).

Van der Hoff [22] reported that the decomposition rate of persulfate is a function of laurate concentration below the CMC. Furthermore, a fixed value of the coagulation coefficient K_f is used for a given monomer system over the whole range of emulsifier concentrations. K_f would be expected to change

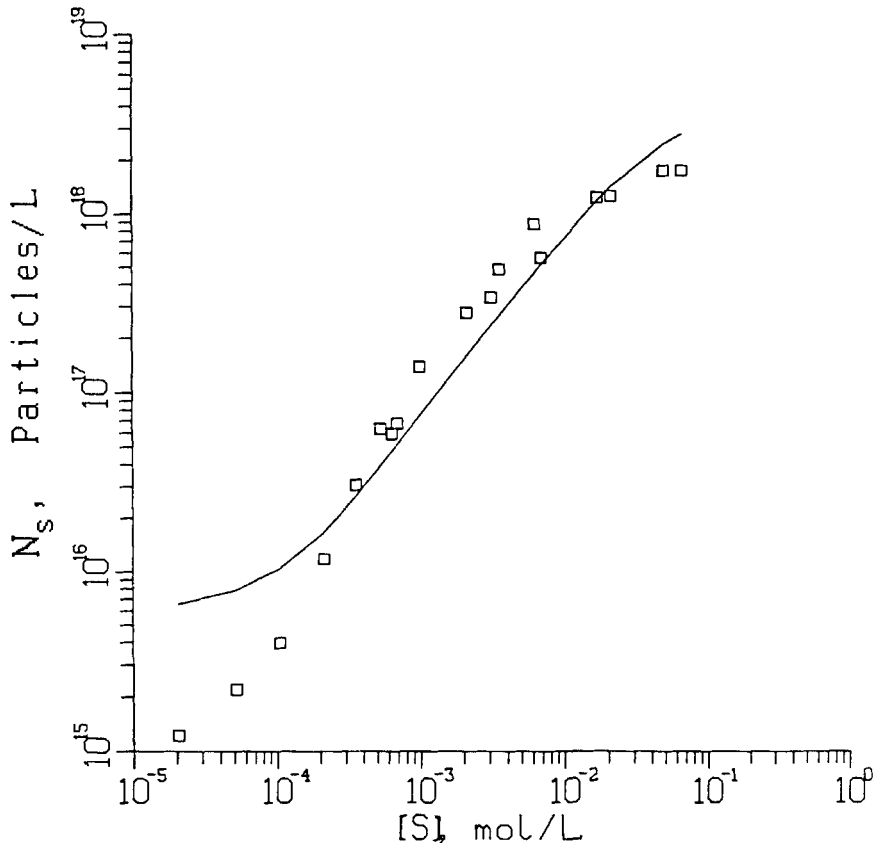

FIG. 24. Variation of the particle number N_s with emulsifier concentration [S] for methyl acrylate at 73°C. Initiator ($(NH_4)_2S_2O_8$), [I] = 0.00635 mol/L. Symbols are experimental data [3]. Curve is from the model prediction with K_f = 2500 L/mol·s, f = 0.3, δ_m = 0.4.

with emulsifier concentration since particle coagulation rates are a measure of latex stability, and latexes are stabilized by emulsifier. In spite of all the simplifications used in estimating model parameters for the simulation, the agreement between model predictions and the experimental data is evident in Figs. 23-30.

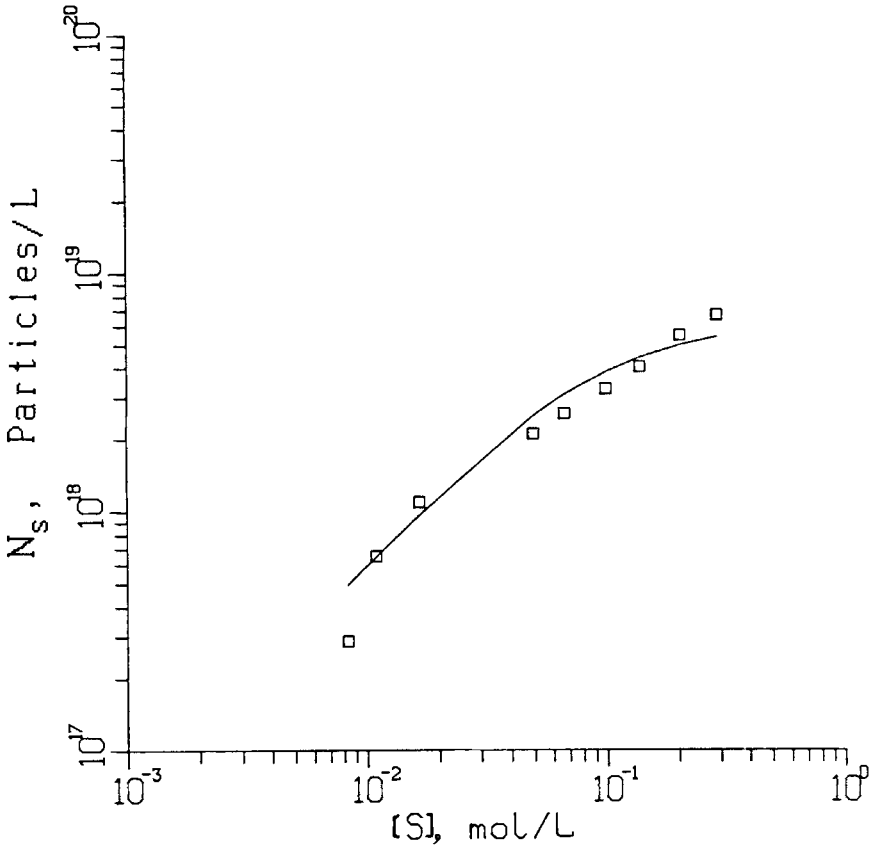

FIG. 25. Variation of the particle number N_s with emulsifier concentration [S] for styrene at 80°C. Initiator ($(NH_4)_2S_2O_8$), [I] = 0.00159 mol/l. Symbols are experimental data [3]. Curve is from the model prediction with K_f = 750 L/mol·s, f = 0.3, δ_m = 0.315.

SUMMARY

The curve of $\log N_s$ vs $\log [Mc]_0$ is of sigmoidal shape with a steep rise around the CMC. When the emulsifier concentration is low, the steady-state particle number, N_s, is governed by homogeneous nucleation, so that N_s in-

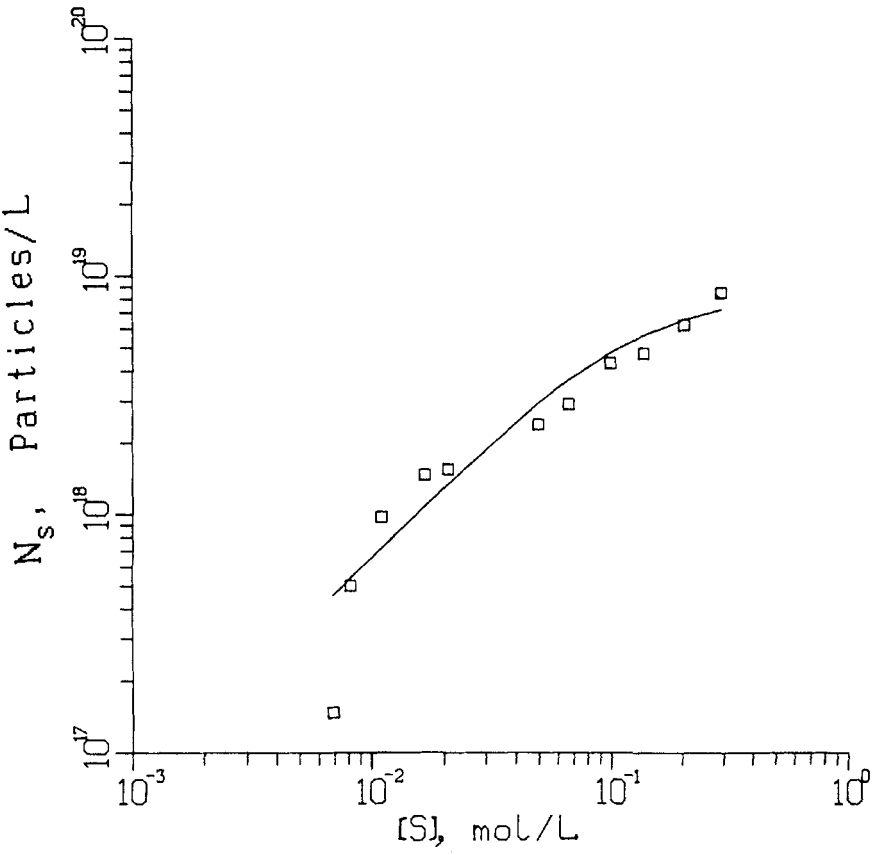

FIG. 26. Variation of the particle number N_s with emulsifier concentration [S] for styrene at 80°C. Initiator ($(NH_4)_2S_2O_8$), [I] = 0.00317 mol/L. Symbols are experimental data [3]. Curve is from the model prediction with K_f = 750 L/mol·s, f = 0.3, δ_m = 0.35.

creases slowly with increasing emulsifier concentration. In this region, N_s increases with increasing polarity of the monomer. The steep rise in N_s with micelle concentration $[Mc]_0$ at higher emulsifier concentrations suggests a transition from domination by homogeneous nucleation to domination by micelle nucleation. The slope of the rising line increases with decreasing rate

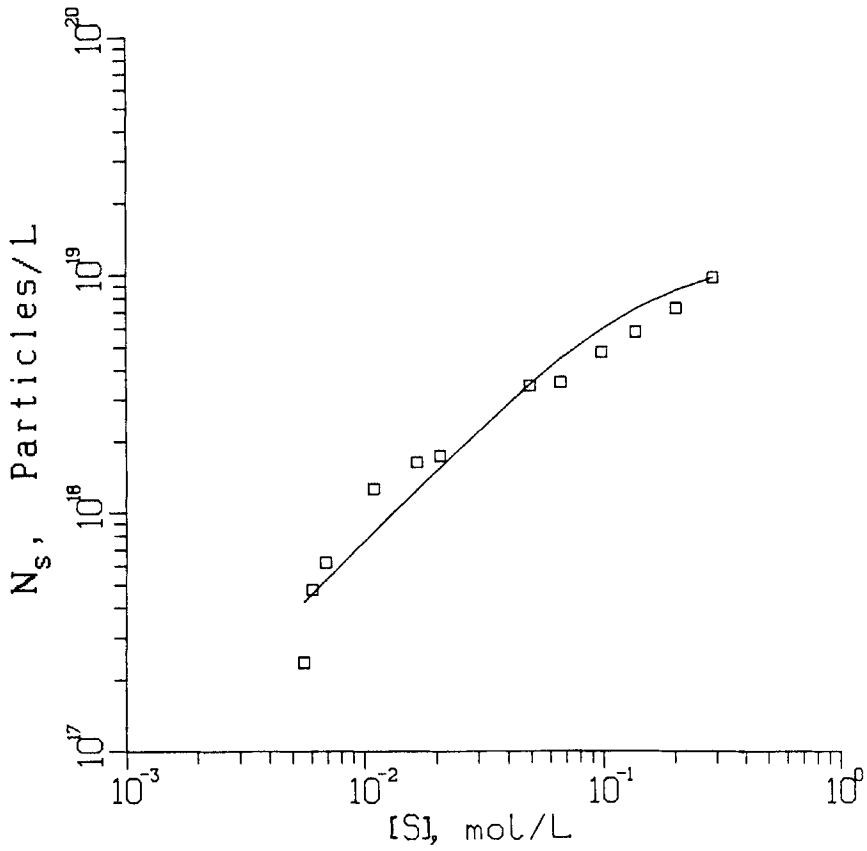

FIG. 27. Variation of the particle number N_s with emulsifier concentration [S] for styrene at 80°C. Initiator ($(NH_4)_2S_2O_8$), [I] = 0.00635 mol/L. Symbols are experimental data [3]. Curve is from the model prediction with K_f = 750 L/mol·s, f = 0.3, δ_m = 0.4.

constant for particle coagulation K_f. Thus the power x of the relationship $N_s \approx [S]^x$ decreases with increasing polarity of the monomer in this region.

When the micelle concentration is high, an insufficient supply of radicals for particle nucleation via micelles and an increasing tendency of particle coagulation due to the increased particle number causes N_s to be independent

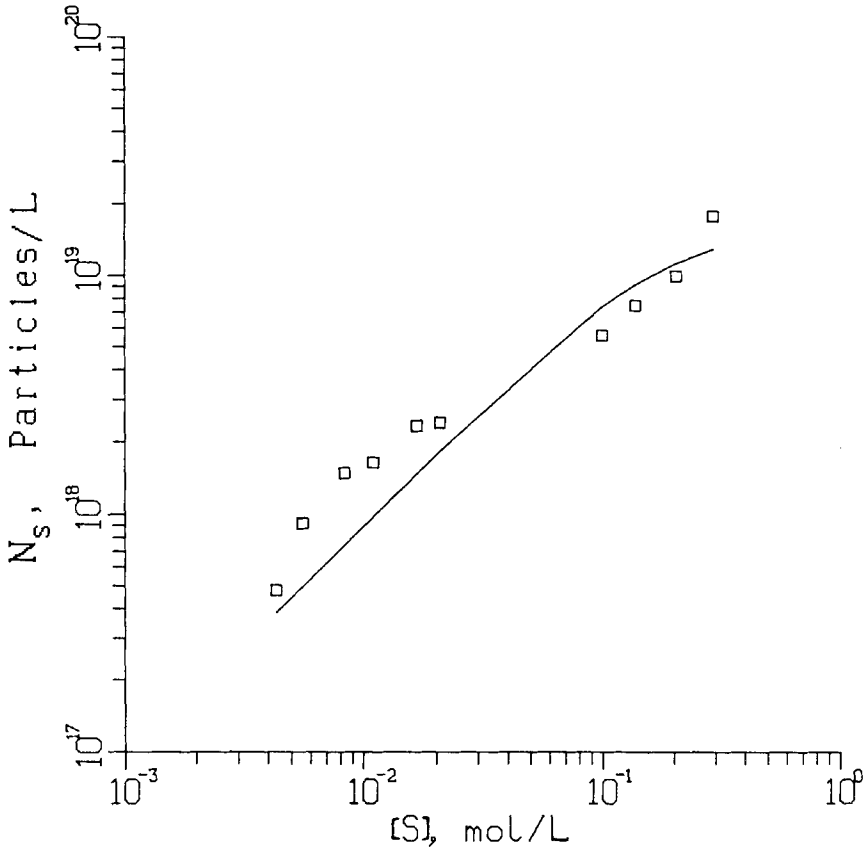

FIG. 28. Variation of the particle number N_s with emulsifier concentration [S] for styrene at 80°C. Initiator ($(NH_4)_2S_2O_8$), [I] = 0.0127 mol/L. Symbols are experimental data [3]. Curve is from the model prediction with Kf = 750 L/mol·s, f = 0.3, δ_m = 0.47.

of emulsifier concentration. These phenomena have also been reported by Vanderhoff [2] and were confirmed by the experimental results presented by Sutterlin [3]. When [S] exceeds the CMC, the particle number increases with increasing initiation rate and then tends to be constant at higher initiation rates.

The model predictions are in general agreement with experimental data

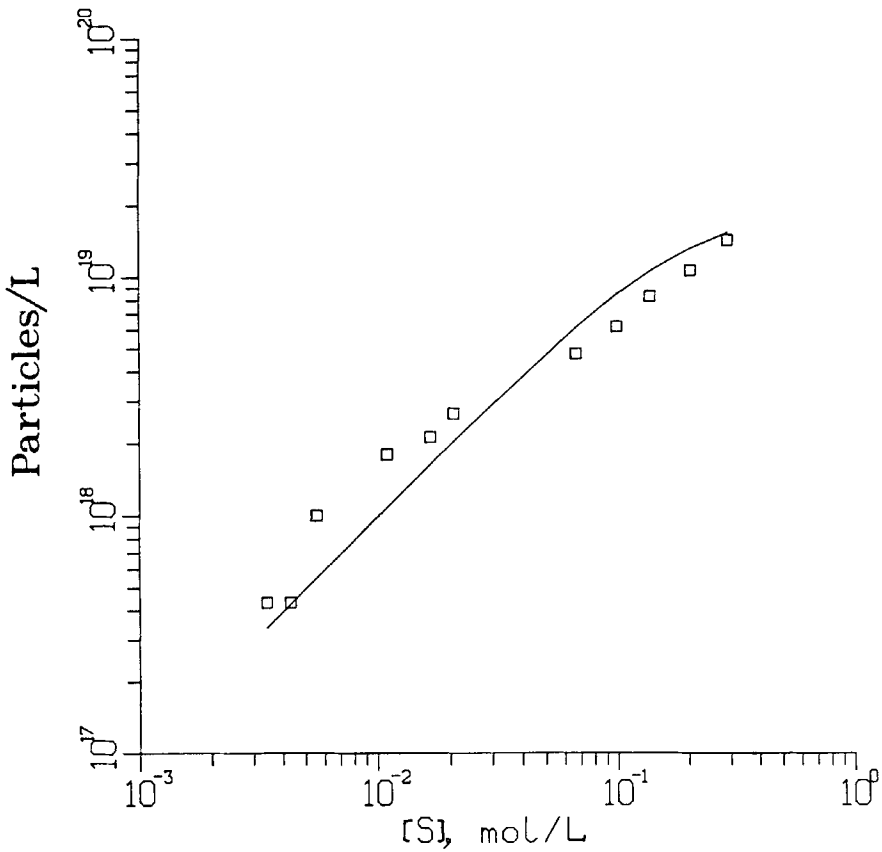

FIG. 29. Variation of the particle number N_s with emulsifier concentration [S] for styrene at 80°C. Initiator ($(NH_4)_2S_2O_8$), [I] = 0.0189 mol/L. Symbols are experimental data [3]. Curve is from the model prediction with K_f = 750 L/mol·s, f = 0.3, δ_m = 0.523.

for various monomers with different water solubility over a wide range of emulsifier and initiator concentrations.

The computer simulation presented in this paper is based on some assumptions (e.g., that D_2 is constant and that chain-transfer reactions can be neglected), and the experimental data used for comparison with model predictions are all based on short-chain anionic surfactants as stabilizers.

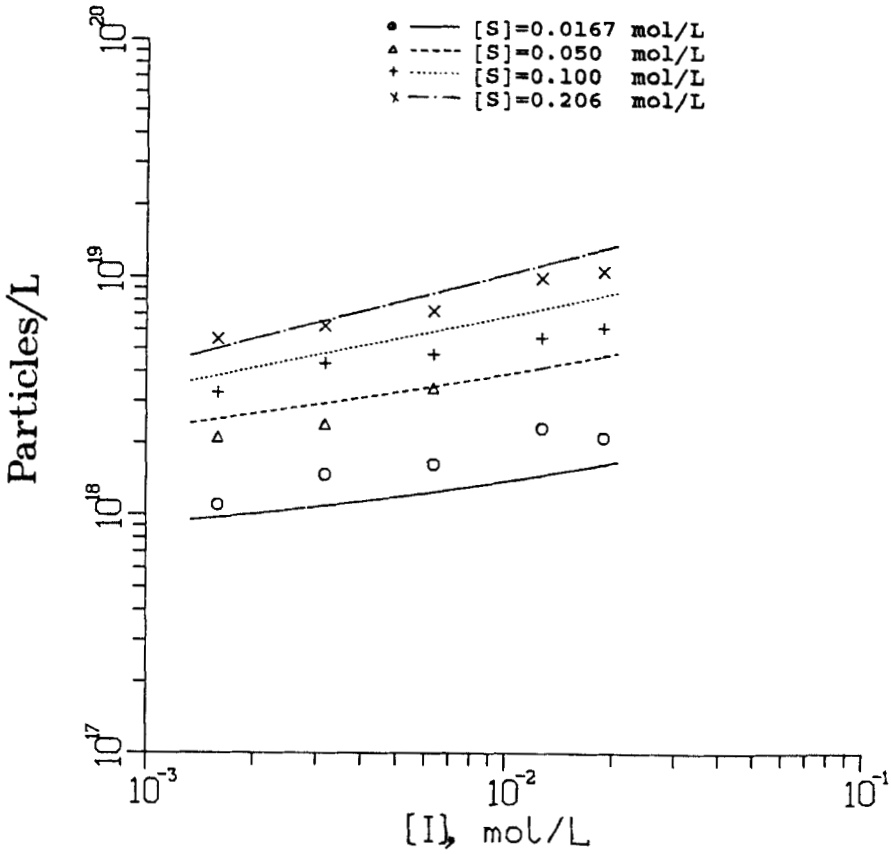

FIG. 30. Variation of the particle number N_s with initiator concentration [I] for styrene at 80°C at different emulsifier concentrations [S]. Symbols are experimental data [3]. Curve is from the model prediction with $K_f = 750$ L/mol•s, $f = 0.3$, $\delta_m = 0.2296 + 2.138[I]^{0.5}$.

Hence, the results might not be applicable to all emulsion polymerization systems.

ACKNOWLEDGMENTS

Financial support from the National Science Foundation under Grant No. CBT-8413987, the Petroleum Research Fund under Grant No. 17638-

AC7, Unocal, Hercules, S. C. Johnson, Dow Chemical, and the Georgia Institute of Technology is sincerely appreciated.

REFERENCES

[1] Z. Song and G. W. Poehlein, *J. Macromol. Sci.–Chem., A25,* 403 (1988).
[2] J. W. Vanderhoff, *J. Polym. Sci., Polym. Symp., 72,* 161 (1985).
[3] N. Sutterlin, in *Polymer Colloids II* (R. M. Fitch, ed.), Plenum, New York, 1980.
[4] W. V. Smith and R. W. Ewart, *J. Chem. Phys., 16,* 592 (1948).
[5] J. W. Breitenbach and H. Edelhauser, *Makromol. Chem., 44-46,* 196 (1961).
[6] M. Morton and H. Landfield, *J. Polym. Sci., 8,* 111 (1952).
[7] N. Friis and L. Nyhagen, *J. Appl. Polym. Sci., 17,* 2311 (1973).
[8] S. Chen and H.-S. Chang, *J. Polym. Sci., Polym. Chem. Ed., 23,* 2615 (1985).
[9] S. P. Chatterjee and M. Banerjee, *Ibid., 16,* 1517 (1978).
[10] R. L. Zollars, *J. Appl. Polym. Sci., 24,* 1353 (1979).
[11] D. E. Moore, *J. Polym. Sci., Part A-1, 5,* 2665 (1967).
[12] I. Piirma, in *Emulsion Polymerization* (I. Piirma and I. Gardon, eds.), (ACS Symp. Ser. 24), American Chemical Society, D.C., 1976.
[13] H. Gerrens and E. Kohnlein, *Z. Elektrochem., 64,* 1199 (1960).
[14] N. Sutterlin, H. J. Kurth, and G. Markert, *Makromol. Chem., 177,* 1549 (1976).
[15] G. Lichti, R. G. Gilbert, and D. H. Napper, *J. Polym. Sci., Polym. Chem. Ed., 21,* 269 (1983).
[16] P. J. Feeny, D. H. Napper, and R. G. Gilbert, *Macromolecules, 17,* 2520 (1984).
[17] D. H. Napper and R. G. Gilbert, *Makromol. Chem., Macromol. Symp., 10/11,* 503 (1987).
[18] A. S. Dunn and S. A. Hassan, *Polym. Mater. Sci. Eng., 54,* 439 (1986).
[19] R. M. Fitch and C. H. Tsai, in *Polymer Colloids* (R. M. Fitch, eds.), Plenum, New York, 1971.
[20] F. J. Bonner, *Prepr. Org. Coatings Plast. Chem., 42,* 181 (1980).
[21] S. Okamura and T. Motoyama, *J. Polym. Sci., 58,* 221 (1962).
[22] B. M. E. Van der Hoff, *Ibid., 48,* 175 (1960).
[23] S. S. Medvedev, *International Symposium on Macromolecular Chemistry,* Pergamon, New York, 1959.
[24] J. Brandrup and E. H. Immergut (eds.), *Polymer Handbook,* 2nd ed., Wiley-Interscience, New York, 1975.

[25] P. L. Flory, *Principle of Polymer Chemistry,* 2nd ed., Wiley-Interscience, New York, 1953, p. 158.
[26] A. R. Goodall and M. C. Wilkinson, in *Polymer Colloids II* (R. M. Fitch, eds.), Plenum, New York, 1980.
[27] F. K. Hansen and J. Ugelstad, *J. Polym. Sci., Polym. Chem. Ed., 16,* 1953 (1978).
[28] G. Odian, *Principle of Polymerization,* 2nd ed., Wiley, 1980, p. 319.
[29] W. J. Priest, *J. Phys. Chem., 56,* 1077 (1952).
[30] Z. Pan, *Polym. Chem.* (*Chinese*), p. 47 (1980).

Received November 25, 1987
Revision received March 7, 1988